Tectonophysics 825 (2022) 229235

Contents lists available at ScienceDirect

Tectonophysics

journal homepage: www.elsevier.com/locate/tecto

The crustal structure in the Northwest Atlantic region from receiver function inversion – Implications for basin dynamics and magmatism

Christian Schiffer [a,*], Alexander L Peace [b], Scott Jess [c,d], Stéphane Rondenay [e]

[a] Department of Earth Sciences, Uppsala University, Villavägen 16, Uppsala 752 36, Sweden
[b] School of Earth, Environment & Society, McMaster University, 1280 Main St W, Hamilton, ON L8S 4L8, Canada
[c] Department of Geoscience, University of Calgary, Calgary, AB, Canada
[d] Department of Chemical and Physical Sciences, University of Toronto Mississauga, Mississauga, ON, Canada
[e] Department of Earth Science, University of Bergen, 5007 Bergen, Norway

ARTICLE INFO

Keywords:
Composition and structure of the continental crust
Seismology
Receiver functions
Joint inversion
Crustal imaging
Rifting
Magmatism

ABSTRACT

The Labrador Sea and Baffin Bay form an extinct Palaeogene oceanic spreading system, divided by a major continental transform, the Davis Strait, with the whole region defined as the Northwest Atlantic. The Davis Strait hosts the Ungava Fault Zone and is the central structural element of the Davis Strait Large Igneous Province (DSIP) that formed broadly coeval with continental breakup to its north and south. While constraints on the crustal structure in this region primarily exist in the offshore, crustal models are limited onshore, which makes an interpretation of regional structures as well as the extent, and therefore origin of the DSIP extremely difficult to ascertain. Here, we have collected all available teleseismic data from the Northwest Atlantic margins and applied a receiver function inversion to retrieve station-wise velocity models of the crust and uppermost mantle. We integrate the outcomes with published controlled-source seismic data and regional crustal models to make inferences about the crustal structure and evolution of the Northwest Atlantic. In particular, we focused on constraining the spatial extent and origin of high velocity lower crust (HVLC), and determining whether it is generically related to the Davis Strait Igneous Province, *syn*-rift exhumed and serpentinised mantle, or pre-existing lower crustal bodies such as metamorphosed lower crust or older serpentinised mantle rocks. The new results allow us to better spatially constrain the DSIP and show the possible spatial extent of igneous-type HVLC across Southwest Greenland, Northwest Greenland and Southeast Baffin Bay. Similarly, we are able to relate some HVLC bodies to possible fossil collision/subduction zones/terrane boundaries, and in some instances to exhumed and serpentinised mantle.

1. Introduction

The Northwest Atlantic, here defined as the Labrador Sea and Baffin Bay (e.g. Abdelmalak et al., 2019), forms an extinct early Cenozoic spreading system separated by the Ungava Fault Zone underlying the Davis Strait bathymetric high (Figs. 1 and 2). The distribution and volumes of breakup-related volcanic products vary considerably along the margins of this region, with first-order variations appearing to be controlled by major faults (Skaarup et al., 2006). Following initial continental rifting, beginning in the Early Cretaceous or possibly earlier (Larsen et al., 2009), the Labrador Sea-Baffin Bay spreading system is thought to have evolved in three stages – Palaeocene, Eocene, and Oligocene to present – including major changes in extension direction (Oakey and Chalmers, 2012). The Labrador Sea-Baffin Bay oceanic basins and rifted margins are heavily segmented both structurally and in terms of igneous products (Skaarup et al., 2006 Abdelmalak et al., 2019; Schiffer et al., 2020; Heron et al., 2019) not least by the Davis Strait, which has acted as a transform between the offset Baffin Bay and Labrador Sea basins and hosts the Davis Strait Igneous Province (DSIP). The DSIP formed largely coeval to continental breakup in the region (Abdelmalak et al., 2019; Clarke and Beutel, 2020). This structural and magmatic segmentation is to a larger degree controlled by pre-existing structures (Peace et al., 2018a; Peace et al., 2018b; Heron et al., 2019; Schiffer et al., 2020), but the dominant mechanism driving continental breakup in the region is debated. This debate specifically focuses on whether a plume played a major role, or whether a plume is even

* Corresponding author.
E-mail address: christian.schiffer@geo.uu.se (C. Schiffer).

https://doi.org/10.1016/j.tecto.2022.229235
Received 29 April 2021; Received in revised form 12 January 2022; Accepted 15 January 2022
Available online 29 January 2022

required to explain breakup, magmatism and structural evolution (Dam et al., 1998; Graham et al., 1998; Peace et al., 2017; Clarke and Beutel, 2020; Foulger et al., 2020; Peace et al., 2020).

While the Northwest Atlantic is well covered by marine deep crustal seismic transects (see references in Fig. 3), seismic constraints onshore are more limited and only available from permanent or temporary seismic stations for earthquake observations and few active source seismic lines (Fig. 3). As a result, onshore-offshore relationships are therefore either poorly or not constrained. Regional crustal models onshore rely on potential field inversion (Welford and Hall, 2013; Welford et al., 2018; Lebedeva-Ivanova et al., 2019), tomographic methods with rather low resolution (e.g. Darbyshire, 2005; Darbyshire et al., 2017; Pourpoint et al., 2018) and only few reference points from previously published station-wise crustal models from receiver function inversion (Dahl-Jensen et al., 2003; Darbyshire, 2003; Kumar et al., 2007; Thompson et al., 2010; Postlethwaite et al., 2014; Dahl-Jensen et al., 2016; Vervaet & Darbyshire, 2022; Gilligan et al., 2016). This is made worse by the extensive ice cover across Greenland, meaning that much of the complex onshore geology remains unmapped (Jess et al., 2020). Information on the crustal structure is essential to constrain the geodynamic evolution of rifting, lithosphere thinning and magmatism, in addition to linking key structures and magmatic volumes from the offshore to the onshore. In particular, high-velocity lower crust (HVLC) in combination with crustal thickness are important constraints for

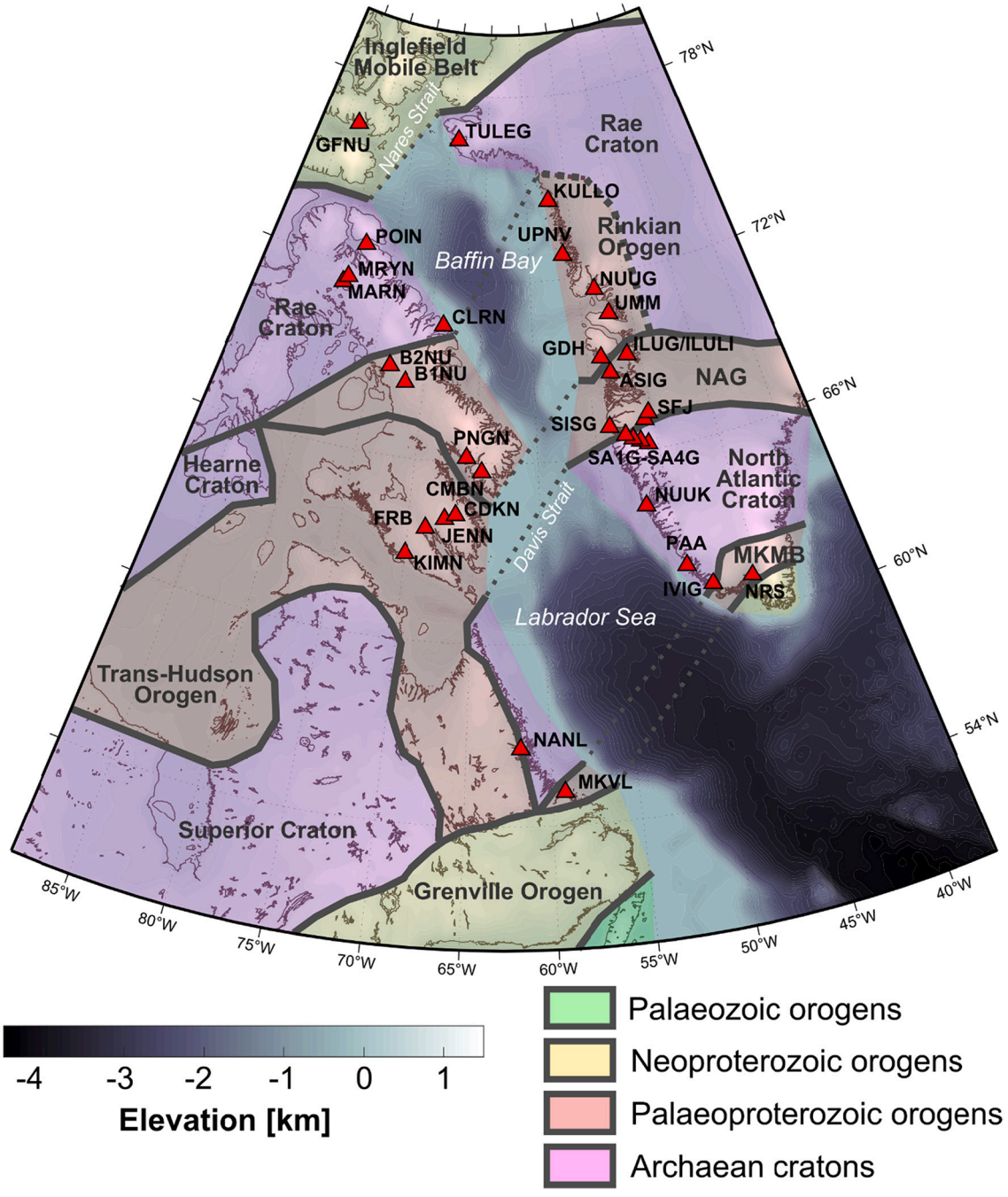

Fig. 1. Simplified, tectonic overview of the major terranes, continental blocks and cratons of the Northwest Atlantic region after St-Onge et al. (2009); Bastow et al. (2015); Schiffer et al. (2020); Corrigan et al. (2021), colour-coded by age. Red triangles mark the seismic stations used in this study. The exact dimensions and boundaries of the Rinkian fold belt (Grocott and McCaffrey, 2017) are not constrained due to ice cover. (For interpretation of the references to colour in this figure legend, the reader is referred to the web version of this article.)

deciphering past geodynamic processes. Moreover, the interpretation of HVLC bodies based on geophysical data is extremely challenging and non-unique, which requires a careful integration with the regional geology.

In this contribution, we present new crustal models from receiver function (RF) inversion using the available passive seismological data in the Northwest Atlantic, including data from many previously unused stations. In particular, our study focuses on the crustal thickness, the nature of the crust-mantle transition, and the presence and thickness of HVLC in the region. These new results are compared to existing regional crustal thickness models (Laske et al., 2013; Welford and Hall, 2013; Welford et al., 2018; Lebedeva-Ivanova et al., 2019) and allow us to update regional models and identify different continental blocks and terranes. Evidence for HVLC will add important onshore information, whilst interpretations of its origin will provide new insight into areas affected by magmatism and structural inheritance to improve our understanding of the Northwest Atlantic rift system and the DSIP. This information will provide new key constraints for geodynamic models of the region (Ady and Whittaker, 2018; Peace, 2021) and, more generally, for models of analogous geological settings elsewhere. Moreover, we will test the hypothesis that plate tectonics, in contrast to dominantly plume processes, have contributed to the formation of the Davis Strait and that part of the HVLC beneath Davis Strait may be related to deformation of a pre-existing metamorphosed crustal keel or metasomatised mantle.

2. Geological setting

2.1. Precambrian

The landmasses surrounding the Northwest Atlantic represent an assemblage of Archean cratons and Proterozoic orogens (St-Onge et al., 2009) which are known to have exerted substantial influence on the subsequent Mesozoic-Cenozoic evolution through the process of structural inheritance (Peace et al., 2018b; Heron et al., 2019; Schiffer et al., 2020). The correlation of Precambrian basement units and tectonic structures across Baffin Bay, Davis Strait and the Labrador Sea has been the focus of previous work (e.g. Kerr et al., 1996; Kerr et al., 1997; Wardle et al., 2002; St-Onge et al., 2009). Nonetheless, substantial unknowns exist, partially due the Greenland Ice Sheet preventing exposure (Jess et al., 2020), but also the Mesozoic-Cenozoic rifting and breakup (Abdelmalak et al., 2019).

The Archean cratons within the Northwest Atlantic are (Fig. 1): the Rae Craton, the Superior Craton and the North Atlantic-Nain Cratons (St-Onge et al., 2009). These cratons are connected by the spatiotemporally and structurally complex Proterozoic Trans-Hudson Orogen (Whitmeyer and Karlstrom, 2007), which comprises reworked Archean crust and juvenile volcanic belts (Whitmeyer and Karlstrom, 2007). The North Atlantic Craton in Greenland is bordered to the north and west by Palaeoproterozoic orogenic belts that are tectonically related to the Trans-Hudson Orogen including the Nagssugtoqidian Orogen (Van Gool et al., 2002; Engström and Klint, 2014; Kolb, 2014), the Rinkian fold belt on the north side (Grocott and McCaffrey, 2017) and the Torngat Orogen on the west side of the craton (Fig. 1) (Scott, 1998). The Nagssugtoqidian Orogen is thought to correlate across Central Greenland, though ice coverage has made this hard to confirm (St-Onge et al., 2009). The Rinkian fold-belt is located on the Baffin Bay margin of West Greenland, but the exact structural relationships and its extent are not completely understood as it is predominantly ice-covered (Fig. 1) (Grocott and McCaffrey, 2017). The Torngat Orogen represents the collision between Nain (part of the North Atlantic craton) and the Core Zone, an assembly of various reworked Archean terranes (Wardle et al., 2002; St-Onge et al., 2009; Corrigan et al., 2021).

Further south, the Palaeoproterozoic Makkovik-Ketilidian Mobile Belt forms the southernmost province north of the Grenville front in Labrador and the southernmost tip of Greenland (Kerr et al., 1996; Garde et al., 2002; McCaffrey et al., 2004; LaFlamme et al., 2013; Dickin, 2021; Hinchey, 2021), while in the northern extreme of the region the Paleoproterozoic Inglefield Mobile Belt is located across North Greenland and Ellesmere Island (St-Onge et al., 2009).

2.2. Formation of the Northwest Atlantic and the davis strait igneous province

The Labrador Sea and Baffin Bay (Fig. 2) formed as a response to the divergence of Greenland and North America. According to Oakey and Chalmers (2012), after early phases of continental rifting (possibly since the Triassic (Larsen et al., 2009), separation occurred in three stages: 1) Separation between North America and Greenland in the Palaeocene, while the latter was still attached to Eurasia; 2) separation between Greenland and North America as well as between Eurasia and Greenland in the Eocene, during which Greenland moved as an independent plate; 3) continued separation between Eurasia and Greenland, which again was attached to North America, since the Oligocene. These main phases of extension resulted in seafloor spreading in the Labrador Sea (Chalmers and Laursen, 1995), and most likely also in Baffin Bay (Suckro et al., 2012). Structural inheritance is inferred to have controlled the compartmentalisation of the Northwest Atlantic highlighting the interaction of pre-existing structures and fabric with oblique rifting (Peace et al., 2018a; Peace et al., 2018b; Heron et al., 2019; Schiffer et al., 2020).

The Davis Strait, where many of the HVLC (high velocity lower crustal) bodies are concentrated, is a bathymetric high linking the Labrador Sea to Baffin Bay that is underlain by crust up to 20 km thick (Funck et al., 2007). The Davis Strait is thought to consist of continental lithosphere (Dalhoff et al., 2006) and hybrid/transitional crust, heavily intruded, as well as patches of exhumed mantle, likely accommodated by the "leaky" Ungava Transform Fault System (Funck et al., 2007; Suckro et al., 2013). Furthermore, the Davis Strait appears to be the centre of Mesozoic-Cenozoic magmatism in the Northwest Atlantic (Funck et al., 2007; Funck et al., 2012; Hosseinpour et al., 2013; Suckro et al., 2013; Abdelmalak et al., 2019). The Davis Strait underwent dextral transtension, but not breakup during the first stage of Labrador Sea-Baffin Bay formation (Wilson et al., 2006; Suckro et al., 2013), followed by further transpression during the second stage (Geoffroy et al., 2001; Suckro et al., 2013).

The earliest magmatism that may be related to extensional processes in the Labrador Sea is Late Triassic in age (ca. 220 Ma; Larsen et al., 2009). However, more significant extensional stresses probably occurred later in the Early Cretaceous, exemplified by coast-parallel dykes in West Greenland (ca. 150 Ma; Larsen et al., 2009), debated equivalents in Labrador (Tappe et al., 2007; Peace et al., 2016), and Mesozoic diatremes (King and McMillan, 1975; Wilton et al., 2002; Wilton et al., 2016).

The majority of the volcanism in the Northwest Atlantic occurred between ~62 and ~ 58 Ma, coincident with an increased spreading rate in the Labrador Sea, and subsequently decreased volcanism after a major change in the spreading direction during the Eocene (~56 Ma), that resulted in a northward drift of Greenland (Oakey and Chalmers, 2012; Abdelmalak et al., 2019) and the Eurekan Orogeny (Heron et al., 2015; Piepjohn et al., 2016; Stephenson et al., 2017). Breakup occurred in the Palaeocene (Chalmers et al., 1995), approximately coeval with the eruption of flood basalt around the Davis Strait (Larsen et al., 2016).

The cause of extension, magmatism, structural complexity and final breakup is debated (e.g. Peace et al., 2017). One proposed model includes a mantle plume (Storey et al., 1998; Courtillot et al., 1999; Nielsen et al., 2002; Funck et al., 2007; Gerlings et al., 2009), while others stress the importance of structural inheritance and plate tectonic processes (Peace et al., 2017; Heron et al., 2019; Clarke and Beutel, 2020; Schiffer et al., 2020). Although geochemical modelling suggests some lavas in the Northwest Atlantic region do require moderately elevated temperatures (up to 1500 °C) with regard to ambient mantle

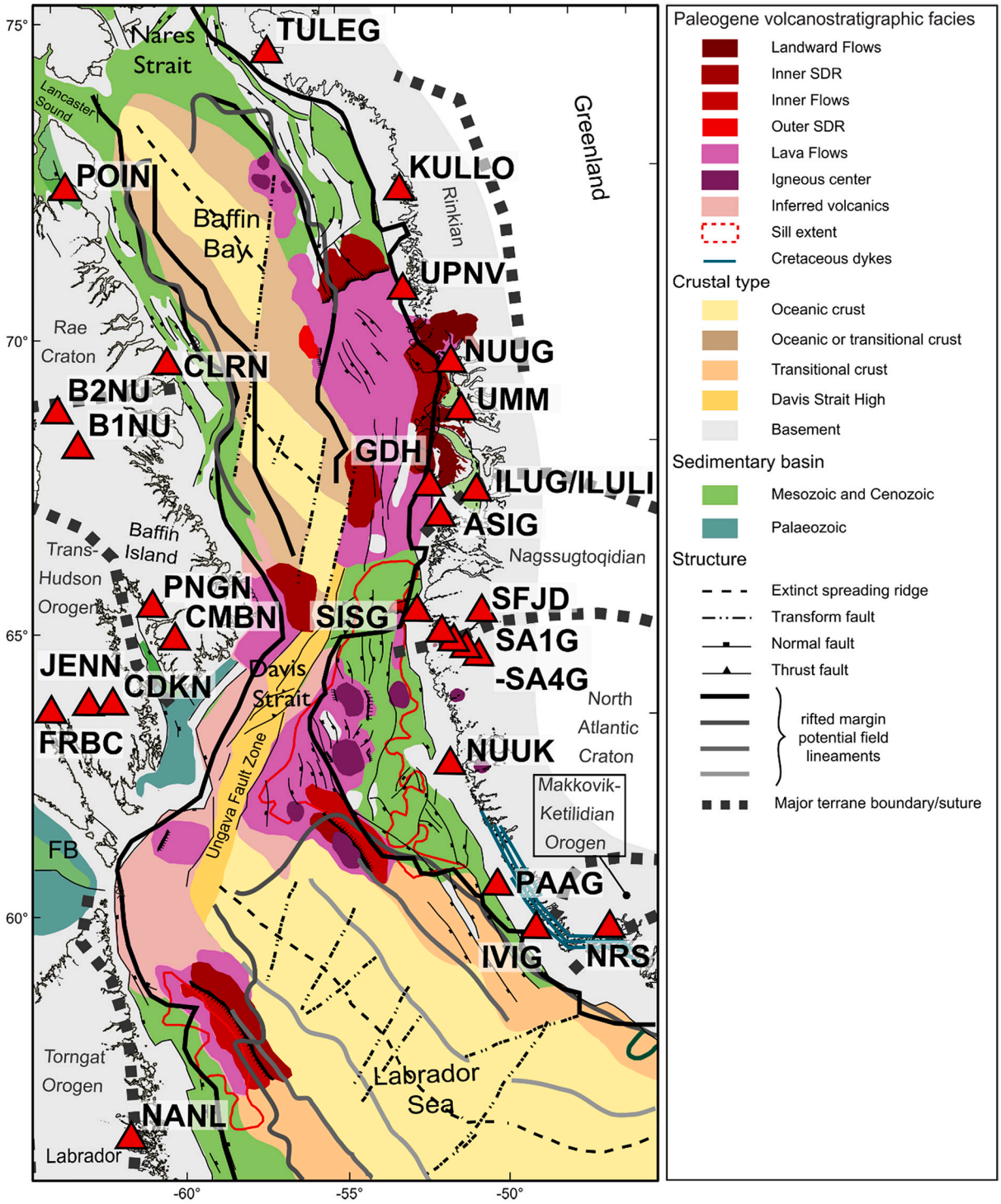

Fig. 2. Tectonic map of the Davis Strait Igneous Province (modified after Abdelmalak et al., 2019) and locations of stations used in this study (red triangles).

temperatures (~1350 °C), deciphering the exact causes of producing these large volumes of lavas is debated (Hole, 2015; Hole and Natland, 2020). The detailed mapping of HVLC and crustal thickness will improve our understanding of the causes and rates of rifting and magmatism in the region.

2.3. Lithospheric structure of the Northwest Atlantic region

Lithospheric structure is vital for unravelling the region's tectonic and magmatic evolution and to reveal the causative mechanisms of rifting, structural segmentation and magmatism. The Northwest Atlantic region has been the subject of various crustal-scale geophysical studies. However, these are primarily located offshore, while detailed information onshore is limited, which led to an unbalanced reporting of detailed crustal structure, for instance the presence of HVLC (see for example Welford and Hall, 2013; Welford et al., 2018 for data overviews).

Information on the lithospheric structure is available from several regional datasets, as well as deep crustal seismic profiles in the Northwest Atlantic region, which we have assembled into maps that illustrate the state of knowledge prior to our study (Fig. 3). The lithosphere-

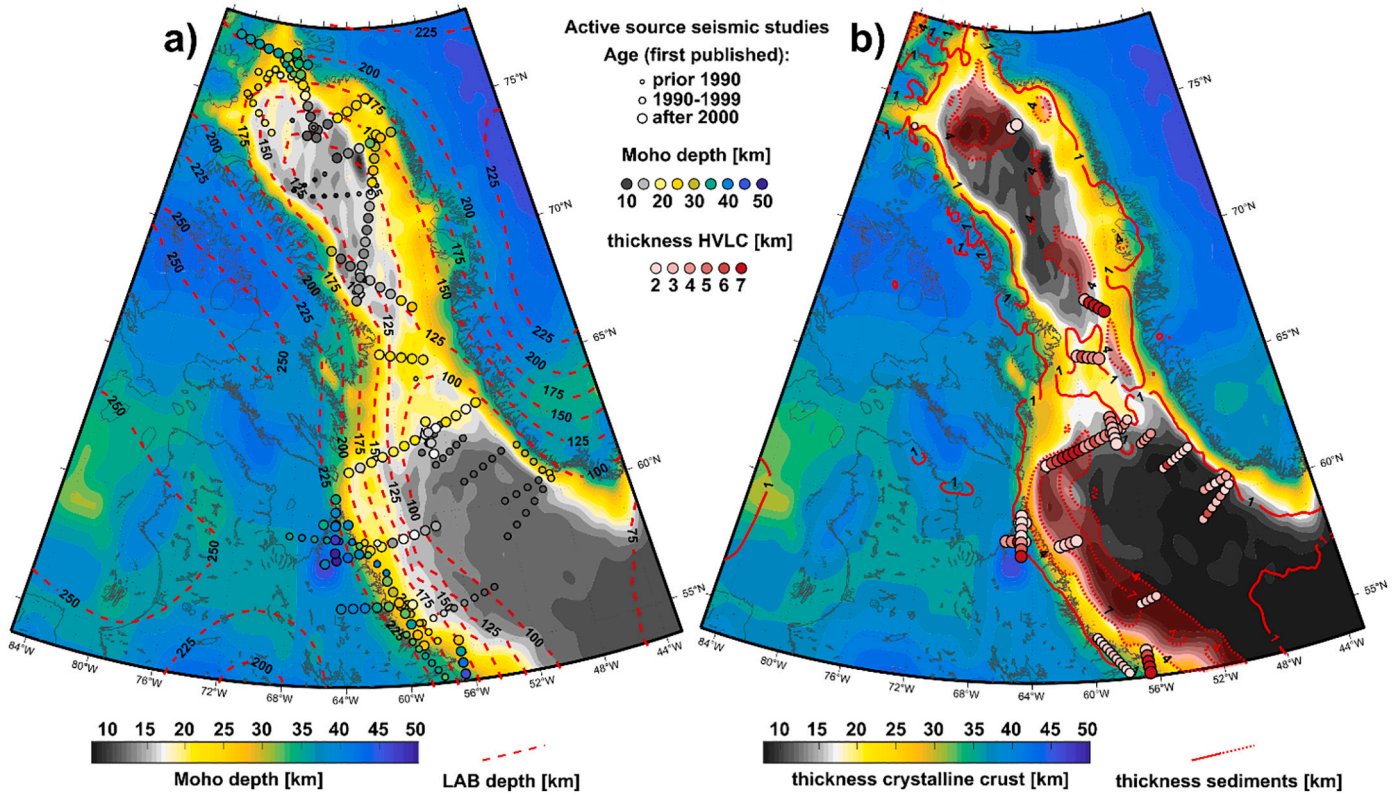

Fig. 3. Lithospheric structure of the Northwest Atlantic region compiled from published regional models and available seismic data. (a) Moho depth (Welford and Hall, 2013; Welford et al., 2018; Lebedeva-Ivanova et al., 2019) (background) and LAB depth (Schiffer and Nielsen, 2016; Schiffer et al., 2018) (red stippled contours). (b) Crustal thickness (background) and sedimentary thickness (red contours and shading) (Welford and Hall, 2013; Welford et al., 2018; Lebedeva-Ivanova et al., 2019). Information from active source seismic models (circles) is compiled from (Keen and Barrett, 1972; Jackson et al., 1979; Chian and Louden, 1992; Chian and Louden, 1994; Jackson and Reid, 1994; Chian et al., 1995b; Reid, 1996; Chalmers, 1997; Reid and Jackson, 1997; Funck and Louden, 1998; Louden and Fan, 1998; Funck and Louden, 1999; Funck et al., 2000a; Funck et al., 2000a; Funck et al., 2001; Hall et al., 2002; Funck et al., 2006; Funck et al., 2007; Funck et al., 2008; Gerlings et al., 2009; Harrison et al., 2011; Funck et al., 2012; Keen et al., 2012; Suckro et al., 2012; Suckro et al., 2013; Altenbernd et al., 2014; Altenbernd et al., 2015; Altenbernd et al., 2016; Keen et al., 2018). (For interpretation of the references to colour in this figure legend, the reader is referred to the web version of this article.)

asthenosphere boundary (Fig. 3a) was presented by Schiffer et al. (2018), which used a seismic tomography model of the Arctic region (Lebedev et al., 2018) showing thick lithosphere of up to 240 km beneath Canada, and up to ~200 km beneath Greenland. The Labrador Sea lithosphere is as thin as 75–120 km, consistent with oceanic lithosphere, while Baffin Bay has a lithospheric thickness of approximately 110–120 km and Davis Strait has the thickest lithosphere (~120 km) in marine areas, although the difference between the latter two is perhaps near resolution limit. Moreover, direct information on the crustal structure is available from a number of crustal-scale seismic refraction and reflection lines mostly in marine areas and some onshore-offshore profiles (see Fig. 3 for list), as well as information from passive source seismology from RFs (Dahl-Jensen et al., 2003; Darbyshire, 2003; Kumar et al., 2007; Thompson et al., 2010; Postlethwaite et al., 2014; Thompson et al., 2015; Vervaet & Darbyshire, 2022; Gilligan et al., 2016) and surface wave tomography (Darbyshire, 2005; Darbyshire et al., 2017; Mordret, 2018; Pourpoint et al., 2018). Information on the crustal structure is taken from Welford and Hall (2013) and Welford et al. (2018) for the offshore areas in Baffin Bay and the Labrador Sea, respectively. Their models are based on gravity inversion with prior information from available seismic data (see Fig. 3 for full list). The circum-Arctic crustal model *ArcCrust* by Lebedeva-Ivanova et al. (2019) gives state-of-the-art information on the crust at latitudes greater than 67°N. For all other areas, we describe the crustal structure based on CRUST1.0 (Laske et al., 2013).

The Moho depth map based on the sources mentioned above (Fig. 3a) shows generally similar trends as the LAB depth model, with thick crust and lithosphere in the cratonic areas and orogenic/mobile belts and thin crust and lithosphere, as expected, in the marine areas. The Labrador Sea has the thinnest crust of ~8–15 km, consistent with a developed ocean basin. Baffin Bay has thicker crust of typically 12–17 km, with local shallow Moho anomalies, while the Davis Strait has the deepest Moho in the range of 17–25 km. Subtracting the sedimentary layers, the crystalline crust (Fig. 3b) in the area shows obvious similarities with the Moho depth and differs mostly in the marine areas, due to water depth and typically thicker sedimentary successions than on land. The distribution of sediments between the passive margins is highly asymmetric, with the deepest basins along the eastern Baffin Bay margin in the north and the western Labrador Sea margin in the south (Peace et al. (2016). The crystalline crustal thickness in the Davis Strait appears to be more complex than the Moho depth, with a N-S oriented convex shaped sliver of thick crust (18–22 km), separated from Baffin Island and West Greenland by two "corridors" of thinner crust. The crustal thickness, structure and velocities observed in the Davis Strait strongly indicate the presence of continental crust and a complex rift development across Davis Strait.

2.4. *High velocity lower crust (HVLC)*

High velocity lower crust (here defined as crustal layers with Vp = ~7.1–7.6 km/s or Vs = ~4.0–4.3 km/s) has been documented across the Northwest Atlantic (summary by Hosseinpour et al., 2013). Knowledge about the type of HVLC is an important constraint for regional geodynamic interpretations, because HVLC can be used as a marker of past

geodynamic processes such as igneous activity, mantle serpentinisation, orogenic events, and mode of crustal formation.

However, unequivocal interpretation of the origin of HVLC is challenging, with much of the ambiguity focused around its composition, formation mechanism and when it was formed (e.g. pre-, *syn*- or post-rift) (Gernigon et al., 2004; Schiffer et al., 2016a; Abdelmalak et al., 2017; Schulte-Pelkum et al., 2017). While HVLC may exhibit uniform geophysical properties (Vs, Vp, density), its origin and composition can be varied (e.g. Gernigon et al., 2004; Schiffer et al., 2016a; Schulte-Pelkum et al., 2017), including syn-rift intruded lower crust (e.g. Thybo and Artemieva, 2013) and exhumed serpentinised mantle (e.g. Péron-Pinvidic and Manatschal, 2009), as well as pre-existing igneous, metamorphic and metasomatised lithologies from previous rifting or orogenic events (e.g. Petersen and Schiffer, 2016). Although hydrated, intruded or otherwise modified peridotite obviously does not actually represent a "lower crustal" lithology, we will include these anomalous bodies at the crust-mantle transition zone in the broad expression "high velocity lower crustal bodies".

Several occurrences of HVLC have been observed in Palaeoproterozoic and/or Archean crust (Schmidt, 2000; Kukkonen et al., 2008; England and Ebbing, 2012; Schulte-Pelkum et al., 2017). In Scandinavia several models have been suggested for this "cratonic HVLC", including the presence of eclogite and lower crustal intrusions/melt residues, but regardless of the mechanism, HVLC must have been emplaced in the Precambrian (Schmidt, 2000; Kukkonen et al., 2008; England and Ebbing, 2012). Schulte-Pelkum et al. (2017) investigated the distribution of HVLC across the continental US based on refraction, RF, tomography and xenolith data. Their results suggest that in some cases HVLC may be specifically related to cratonic crustal domains, as the thickest occurrences were observed in Proterozoic crust from the central and eastern US, while HVLC was not present in other cratonic areas. Also, according to the authors, the formation and destruction of HVLC could have happened at any time since its emplacement and through several distinct events. Areas of younger tectonic age exhibit only thin HVLC, which has led to the suggestion that HVLC formation may relate to periods when conditions are favourable for garnet growth. Although cratonic-type HVLC has been observed under many continents, important questions remain regarding its formation mechanism and how widespread it is globally.

The available regional crustal models from the Northwest Atlantic (Welford and Hall, 2013; Welford et al., 2018; Lebedeva-Ivanova et al., 2019) do not describe an additional layer for HVLC, but HVLC has been mapped in the Northwest Atlantic by deep seismic studies (see Fig. 3 for references). Hence, we extract information on the presence and thickness of HVLC directly from the original publications, typically from refraction seismic lines (i.e., by identifying lower-crustal layers with Vp = 7.1–7.6 km/s, Fig. 3b). We find that HVLC is abundant along the Labrador Sea margins (Chian et al., 1995b; Chalmers, 1997; Chian et al., 1998; Keen et al., 2018), reaching thicknesses of 6 km, but usually in the range of 2–4 km. Here, these lower crustal bodies are typically interpreted as *syn*-rift exhumed and serpentinised mantle. However, on the northernmost West Greenland Labrador Sea margin, close to the Davis Strait, newer seismic data suggests that these structures belong to a larger system of HVLC that is likely of igneous nature (Funck et al., 2007; Gerlings et al., 2009). Also, several of these HVLC bodies are within the spatial confines of the Davis Strait Igneous Province (DSIP) (Fig. 2 and 3) or in very close vicinity, which makes an igneous nature likely, as interpreted by Hosseinpour et al. (2013). Therefore, the HVLC along the Labrador Sea margins requires a thorough and targeted investigation with full reconsideration of a possible magmatic origin. The Davis Strait shows evidence for HVLC of up to 8 km thickness over a length of 300 km along the bathymetric high (Funck et al., 2007; Gerlings et al., 2009). The northern extent cannot be established based on the available seismic data, but to the south the HVLC appears to terminate when entering the oceanic domain (Gerlings et al., 2009). It is likely that this igneous HVLC extends further north to the northern limit of the Davis Strait, where Suckro et al. (2013) found HVLC of up to 5–6 km thick and 175 km wide. HVLC up to 8 km thick has been found offshore Disko Island, while the eastern (landward) limit of this HVLC body was out of range (Funck et al., 2012). In northern Baffin Bay, there is minimal evidence for HVLC. Specifically, Harrison et al. (2011) document HVLC at one location in Lancaster Sound, and Altenbernd et al. (2014) inferred a small HVLC body from a refraction seismic line south of the Thule airbase in Northwest Greenland. However, all other seismic lines in this area do not show evidence for HVLC (see comparison between Fig. 3a and b). Information on the presence of HVLC is limited to the deep seismic lines, while one can only infer the spatial extent between these, and no or only little information is available in the onshore areas.

Funck et al. (2000b) report a thick HVLC keel in the northern Torngat Orogen, northern Labrador. This same structure was previously imaged by Funck and Louden (1999), who interpreted the high velocity crustal keel to have formed during the collision of the North Atlantic Craton with the Core Zone as part of the Trans-Hudson Orogeny. These seismic studies also suggest that the Palaeoproterozoic crust to the west of the Torngat Orogen has a HVLC layer. Louden and Fan (1998) and Funck et al. (2001) reported thick HVLC of up to 20 km in the northeastern Grenville Province (the southernmost limit of our study area) and related these to a magmatic body originating from late Precambrian Iapetan rifting, underthrusted beneath Precambrian crust and possible additional metamorphosed lower crust.

The HVLC imaged in the offshore domain of the Northwest Atlantic by previous studies has mostly been interpreted as mafic lower crustal intrusions, predominantly in the Davis Strait area, or syn-rift exhumed and serpentinised mantle along the Labrador Sea margins. Hosseinpour et al. (2013) published an interpretation of the extent of HVLC related to Palaeogene magmatism and included some of the Labrador Sea seismic profiles that were previously considered representing exhumed mantle (Chian and Louden, 1994; Chian et al., 1995b; Chalmers, 1997).

Interpretation of geophysical data is generally non-unique, and this is especially the case for HVLC bodies, which frequently show similar seismic properties and densities irrespective of origin. Nonetheless, determining the origin of HVLC is of utmost concern in understanding the geologic evolution of such regions. Usually, only through interpretation of complementary high-resolution geophysical datasets (e.g. reflection, Vp and Vs refraction, gravity, magnetics) and good controls on structure, evolution, HVLC morphology and a combination of geophysical properties, can HVLC be interpreted with more certainty. In the case of the Northwest Atlantic, the seismic data are of various age, quality and type, usually with little complementary information, which often results in uncertainty and ambiguity in interpretation of the HVLC. The point-wise one-dimensional crustal models from RF inversion have the additional problem that these cannot be brought into a two- or three-dimensional structural context.

The existing models, as well as the sparse and uneven distribution of data, illustrate the need for additional constraints to make stronger inferences about the structural and magmatic evolution of the region. Our interpretations are limited to regional correlation with Moho depth estimates, known structures and lineaments, as well as the distribution of volcanics in the region. The DSIP is the central element in the Northwest Atlantic that we base most of our inferences of igneous-type HVLC on. Additionally, there is evidence for Cretaceous magmatism along the Labrador Sea margins (Tappe et al., 2007; Larsen et al., 2009; Peace et al., 2016). The region is also crossed by numerous terrane boundaries and sutures (St-Onge et al., 2009), many of which have been reactivated during breakup of the Northwest Atlantic (Schiffer et al., 2020, Peace et al., 2018a, 2018b). The Davis Strait is underlain by continental crust and lithosphere (Fig. 3) and has likely formed in response to rift interaction with pre-existing lithospheric scale structures (Peace et al., 2018a; Heron et al., 2019). We know from numerical models that pre-existing structure and thermal regime can lead to lower crustal flow, deformation of pre-existing metamorphic complexes and magmatic budget (Petersen and Schiffer, 2016; Petersen et al., 2018). For example,

recent models propose the Greenland-Iceland-Faroes Ridge to be formed by reactivation of pre-existing structures and flow of thickened and soft continental lower crust to form a continual ridge crossing the Northeast Atlantic Ocean, possibly due to interaction of propagating rifts and different pre-existing orogenic fabric (Schiffer et al., 2015b; Petersen et al., 2018; Foulger et al., 2020; Schiffer et al., 2020).

3. Receiver function modelling

RF analysis is a well-established seismological technique to investigate crustal and upper mantle discontinuities, as well as seismic properties of the subsurface (e.g. Ammon et al., 1990; Cassidy and Ellis, 1993; Kind et al., 1995; Owens et al., 1987; Sandvol et al., 1998). The RF method provides estimates of the Earth's impulse response by deconvolving the incident P-wavefield of teleseismic earthquakes (30–90 degrees epicentral distance) from the P-to-S (Ps) converted wavefield (Vinnik, 1977; Langston, 1979). Deconvolution equalises source and path effects, as well as the instrument response, to represent the Ps conversions as isolated pulses in time (Clayton and Wiggins, 1976; Langston, 1979; Ammon, 1991). An RF consists of the superimposition of the primary conversion of every interface (Ps) and multiple "echoes" of these interfaces (e.g., reflections/conversions of downward propagating waves reflected at the free surface, PpPs, PsPs and PpSs). In cases of multi-layer models, multiples from shallower layers overprint and potentially disturb the primary conversions at deeper discontinuities and need to be considered in modelling. Inverse modelling of stacked RF waveforms provides one-dimensional crustal seismic velocity models beneath the recording stations (Owens et al., 1987; Ammon et al., 1990; Cassidy and Ellis, 1993; Sandvol et al., 1998; Darbyshire, 2003; Ottemöller and Midzi, 2003). RFs can also be jointly inverted with complementary seismological information such as surface waves and incident wave polarisations (e.g. Julià et al., 2000; Kiselev et al., 2008; Schiffer et al., 2019).

Here, we obtain 1D velocity models of the crust and uppermost mantle, by simultaneously inverting two datasets produced from the raw three-component seismograms: P-receiver functions and P-wave polarisations. We generate P-receiver functions using water level deconvolution (Clayton and Wiggins, 1976; Langston, 1979; Ammon, 1991) applying a gaussian factor of 2.5 for low-pass filtering. The dominant frequency of the RF signal is ~1 Hz, resulting in a theoretical vertical resolution for converted waves of ~4 km at Moho depth (assuming a resolution of 1/2 wavelength and velocities of 7–8 km/s, e.g. Bostock, 1999; Rychert et al., 2007). The water level in the deconvolution is chosen to suppress noise (high water-level for noisier data), but it also has the unwanted effect of suppressing some of the actual signal, especially at higher frequencies. Special care must thus be taken to select an optimal water level. This can either be done subjectively via trial and error (here with values of 0.1 or 0.01, depending on the noise level), or objectively by basing the water level on the pre-event noise of the vertical component as is done in the GLImER database workflow of Rondenay et al. (2017). All RFs at each station were averaged and no moveout correction was applied, as this would distort either of the primary or multiple phases and we regard the simple stack of RF waveforms as the best compromise.

The second dataset, the polarisation of incident teleseismic P-waves, provides information on the absolute S-wave velocity distribution in the shallow subsurface (Svenningsen and Jacobsen, 2007). This information is retrieved from the ratio of the radial (R) to the vertical (Z) RFs, i.e., R-RF/Z-RF, at zero delay time of the RFs (Svenningsen and Jacobsen, 2007). The obtained velocities are in fact apparent velocities (Vs_{app}) of the vertical velocity structure, covered by the dominant wavelength of the incident wave. Using increasing periods/wavelengths of the incident waveform, these apparent velocities capture greater depths beneath the recording stations, which then can be inverted to obtain an absolute velocity model with depth. This principle has recently been applied to both onshore and offshore studies (Schiffer et al., 2015a; Hannemann et al., 2016; Schiffer et al., 2016b; Chong et al., 2018). We produce curves of Vs_{app} at increasing periods (T), following the procedure by Svenningsen and Jacobsen (2007). Each individual RF is used to calculate distinct $Vs_{app}(T)$ curves, while the median curve is considered to give the most robust representation. The periods are defined as a set of 26 discrete values on a logarithmic scale from 1 to 25 s, which corresponds to approximately 1–200 km depth range (assuming a minimum Vs of 1 km/s and a maximum of 8 km/s). The data error is given as the standard deviation of the 68% $Vs_{app}(T)$-curves closest to the median.

The employed inverse algorithm is based on the one presented in Schiffer et al. (2019) and previous versions (Schiffer et al., 2015a, 2016b), but with major modifications. In the present study, we combine a linearised iterative least squares inversion as in previous publications of the authors applying (based on Tarantola and Valette, 1982; Menke, 1989; Ammon et al., 1990) with a new random model search scheme. For every station, 1000 full linearised iterative LSQ inversion runs were calculated with a minimum of 15 iterations and vastly different starting models, randomly covering the parameter space. Each starting model has a randomly chosen velocity distribution (between Vs = 1 and Vs = 5 km/s) and a randomly varying number of layers (between 5 and 20) and layer thicknesses, with the only imposed restrictions being that each starting model is monotonically increasing in velocity with depth and that the lowermost layer must have a Vs larger than 4.2 km/s.

The synthetic waveforms are calculated from the 1-D velocity models with the method of Kennett (1983), deconvolved using water-level deconvolution (Clayton and Wiggins, 1976; Langston, 1979; Ammon, 1991) and finally convolved with the observed teleseismic wavelet (deconvolved longitudinal (L-) component – the component rotated and pointing in the direction of the apparent incidence angle using the Vs_{app} at the lowest period of 1 s) to simulate the full RF response for every forward model with all its complexity. Synthetic Vs_{app} is calculated from the synthetic Z- and R-components.

Each individual inversion yields a model and data error (Qd and Qm) defined as the root mean square errors relative to the starting model and observed data, weighted with the respective prior uncertainties (based on observed data covariances). There is also an additional roughness error (Qr), defined by the second derivative of the velocity model. The sum of these error terms results in a total error Q (see Schiffer et al. (2016b) for details).

For each of the 1000 individual inversion runs, the 10 last iterations before termination of the inversion are saved, resulting in a total of 10,000 models forming a posterior model population. Depending on starting model and data quality, the speed of convergence and the number of iterations needed to reach convergence differs. If the data are "less non-unique", show little noise, and the underlying geology is simple, the inversion should effectively converge, which means that the last 10 saved iterations should be very similar. Vice versa, if the data are non-unique, noisy, and reflect a very complex subsurface the inversion may not effectively converge, in which case the last 10 iterations may represent a much larger spread of velocity models. Taking an average model of these 10 hypothetical solutions will result in a small and large posterior model error (or model uncertainty), respectively.

The RFs are modelled from −1 to 20 s delay time with respect to the direct P-arrival at 0 s and Vs_{app} at periods from 1 to 25 s. A priori data errors based on the independent data covariance matrices are used to automatically weigh the individual datasets. That is, if one dataset shows a larger spread, the observed error is large and the weight of the respective dataset is reduced in the inversion. Velocities and depths/delay times are virtually unconstrained in the inversion, meaning that both model parameters can freely change without causing any model error, with one exception: the lowermost mantle half-space velocity is tied to a velocity of Vs = 4.6 km/s by an a priori model error of 0.2 km/s, forcing the lowermost velocity to settle around "ambient mantle" velocities.

The non-uniqueness of the inverse problem is reduced by parameterising layers in terms of delay-time instead of thickness (Jacobsen and

Svenningsen, 2008). RF inversion is primarily sensitive to Vs, but requires Vp model parameters, which mainly affect the delay time of Ps phases. In our approach, the inversion is not technically estimating Vp as an independent model parameter, but Vp is coupled to Vs by a predefined Vs-dependent Vp/Vs ratio lookup table, roughly based on common lithologies (Christensen, 1996) in the following way: We employ increasing Vp/Vs ratios with decreasing Vs below 3.0 km/s with a maximum of 1.85 at 1 km/s. For Vs = 3.0–3.5 km/s we use a Vp/Vs ratio of 1.73. Above Vs = 3.5 km/s, the Vp/Vs ratios increase to a peak of 1.8 at 4.1 km/s, after which they decrease again to 1.75 at 4.6 km/s. For

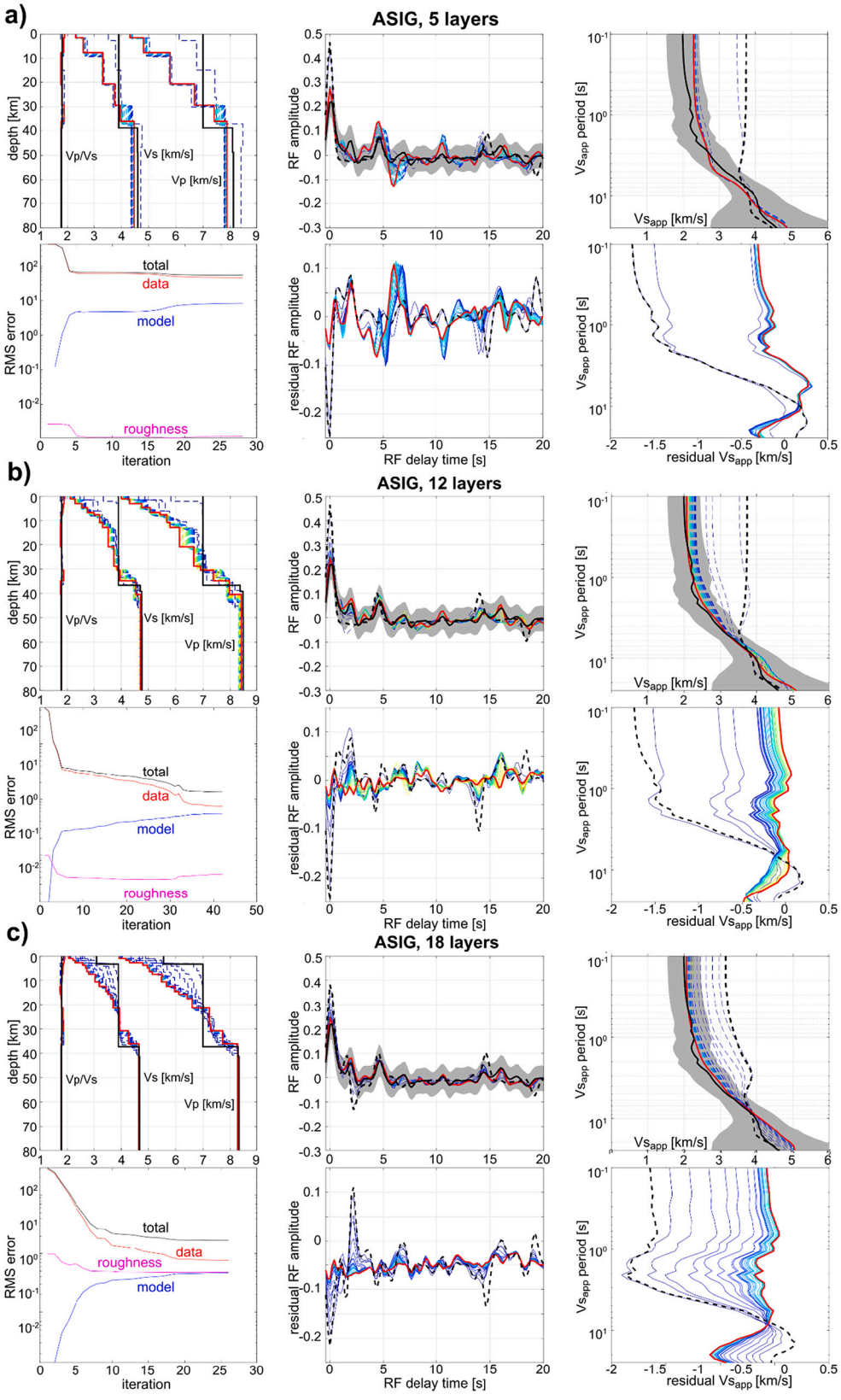

Fig. 4. Example linearised LSQ inversion of station ASIG with 5 (a), 12 (b) and 18 (c) layers. Each panel consists of 6 plots showing the progression of data, models and errors through iterations. Generally, for all subplots except the bottom left (errors), black lines indicate the starting model or observed data, red lines indicate the final model and the corresponding synthetic data or data misfit, stippled black lines show the synthetic data/data misfit of the starting model, rainbow colour scheme illustrates the progression with iteration (blue-green-yellow-orange-red from early to late iterations). Top left: Development of the velocity model; top centre: development of the RF data (rainbow colours – blue early models, red late models) in comparison to the observed data (black); top right: development of the Vs_{app} data; bottom left: development of the total and individual errors (data, model, roughness); bottom centre: development of the RF data misfit; bottom right: development of the Vs_{app} data misfit. (For interpretation of the references to colour in this figure legend, the reader is referred to the web version of this article.)

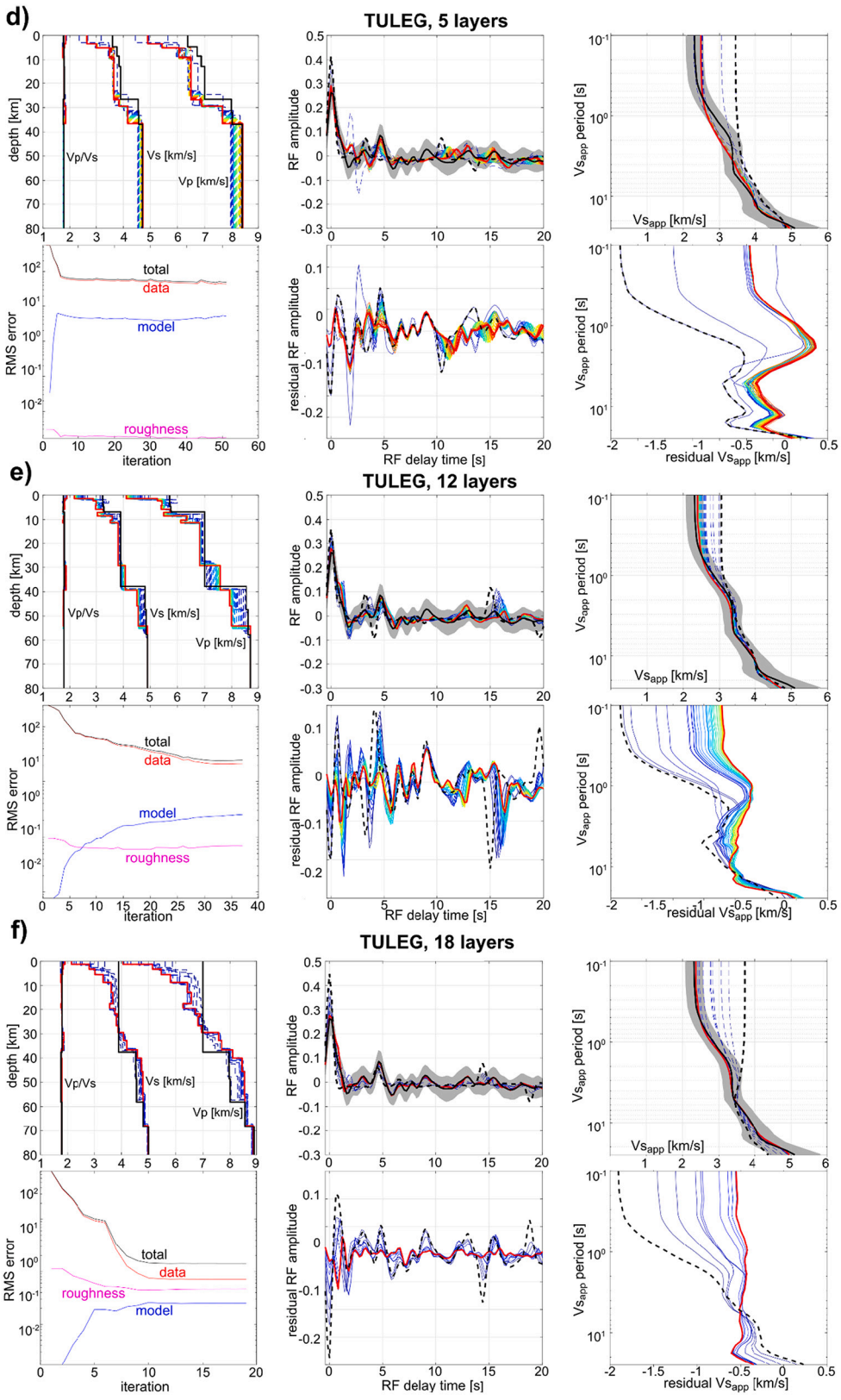

Fig. 4. (*continued*).

Vs > 4.6, the Vp/Vs ratios increase and plateau at a Vp/Vs of 1.78.

Such an approximation can obviously not account for overlaps between seismic parameters of different lithologies and also doesn't capture all lithologies, for example basalts, quartz-rich, dry sedimentary rocks or evaporites. However, using such an approximate Vp-Vs relationship stabilises the inversion immensely. Densities are calculated from Vp at different depth (Christensen and Mooney, 1995).

Examples of the progression of an iterative inversion for one starting model is shown in Fig. 4. The error is usually reduced at each iteration of the inversion, which ends when the models and errors converge, i.e.

changes of less than 1% are observed for more than 2 iterations.

4. Seismological data

We collected passive, broadband, three-component seismological data from various public sources. Raw data from 24 stations were collected through the data services of EIDA (http://www.orfeus-eu.org/data/eida/), IRIS (http://service.iris.edu/) and the Canadian National Data Centre (CNDC). The stations belong to POLARIS network, the Canadian National Seismic Network, the Danish Seismological Network, and other temporary networks used in previous studies (e.g. Dahl-Jensen et al., 2003; Darbyshire, 2003; Kumar et al., 2007; Gilligan et al., 2016; Darbyshire et al., 2017). For the closely spaced, temporally separated stations ILULI and ILUG, we combined the data and refer to the resulting dataset as ILUG/ILULI in the following. Computed receiver functions from 10 temporary stations in West Greenland were retrieved from the global receiver function database GLImER (Rondenay et al., 2017). Depending on recording time and data quality, the various stations yielded between 9 and 448 processable events that had magnitudes between 5.1 and 9.1 and were located in the teleseismic distance ranges (30–90° epicentral distance). This resulted in a total dataset of 3490 events for all stations (~103 events on average per station) that was used for further RF/P-wave polarisation processing and inversion.

5. Crustal model interpretation

The applied inverse approach produces a distribution of 10,000 models for each station. A model histogram is created from these 10,000 models, where every model is weighted with the inverse data error, giving a higher count to models with a better data fit (Fig. 5). The final model is defined as the mean of the weighted population at every depth.

Although the model describes the vertical velocity structure of the entire crust and the uppermost mantle (according to the assumptions, approximations, limitations and inverse procedure described), our study focusses on two specific measures of crustal structure: 1) the crust-mantle transition, and 2) the thickness of HVLC.

Several challenges in interpreting the nature and structure of the crust-mantle transition using the 1D models were encountered. Our interpretation is based on the assumption that the lithospheric stratification beneath the stations is one-dimensional, which likely presents an oversimplification of the structure. However, in the presence of only minor three-dimensional variations in a radius of ~10–15 km around a

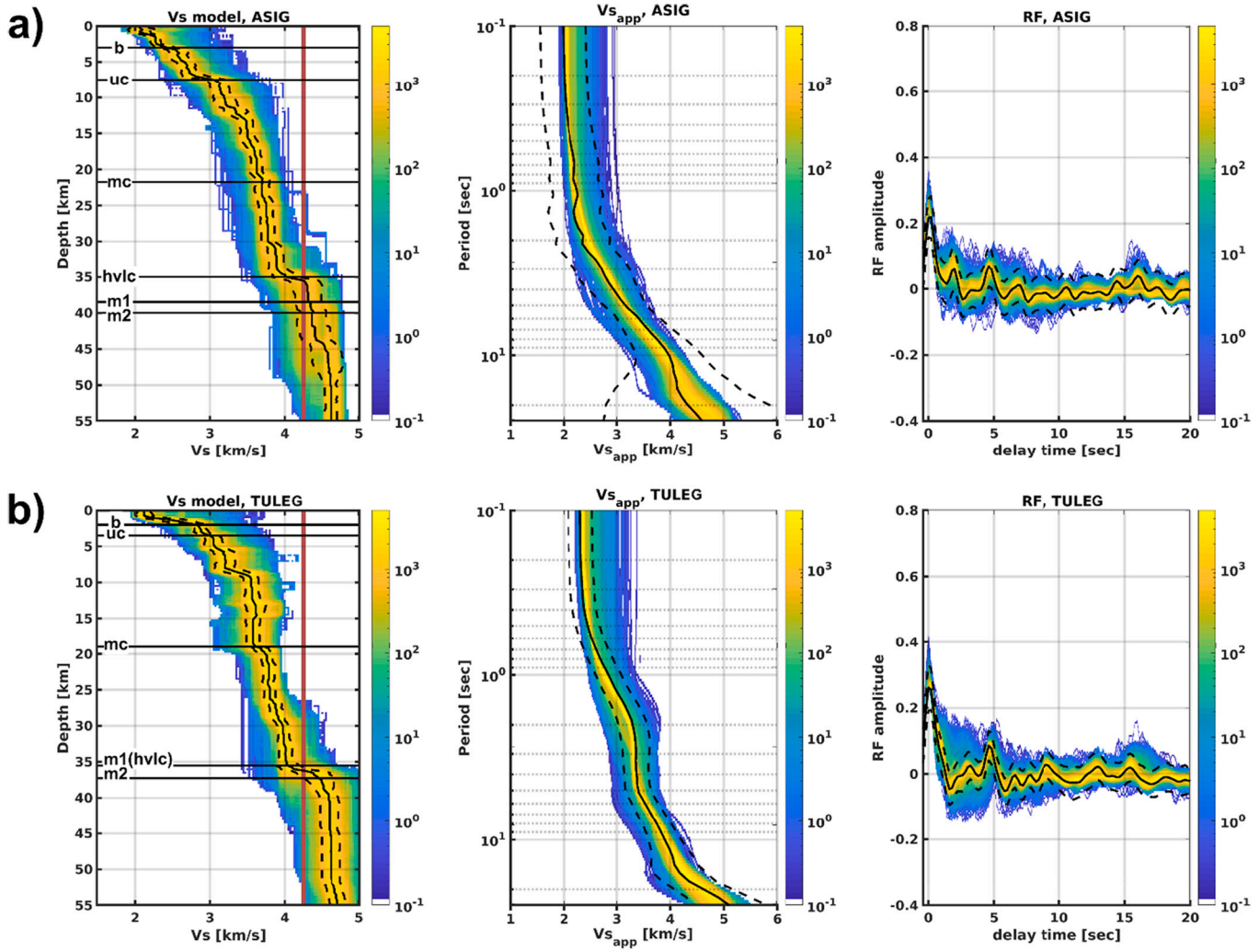

Fig. 5. Inversion results for station ASIG (a) and TULEG (b), showing the 10,000 posterior models weighted with their RMS error. Left: S-wave velocity models; centre: Vs_{app} curves; right; RF waveforms. The final model is defined as the mean of the model population. The model uncertainty is defined as the 95% confidence interval of the model population. Horizontal black lines indicate major layer interpretations, such as basement (b), uppermost crust (uc), mid-crustal discontinuity (mc), top of the high velocity lower crust (hvlc), and top and bottom of the Moho transition (m1 and m2), if observed. The vertical red line indicates the typical division between crustal and mantle velocities, although this boundary is not rigid and is only used as a guideline. (For interpretation of the references to colour in this figure legend, the reader is referred to the web version of this article.)

station this is a reasonable assumption at the scale of the interpretation (e.g. Rondenay, 2009). In the case of highly variable crustal architecture beneath a station, the RF stack will represent an average of the different individual waveforms and, hence, the obtained model will similarly be a representation of this averaged waveform. Experience shows that in the presence of lateral structural gradients, for example in Moho depth, sharp discontinuities will start to appear smoother in the waveforms due to stacking of the converted phase at different delay times, as well as in the obtained velocity model. In other words, a sharp, but substantially dipping discontinuity may appear as a velocity gradient.

This potential issue also affects the interpretation of the HVLC layer. An apparent Moho gradient and/or HVLC-like velocities may be real, but could also be the effect of this smearing in the presence of strong lateral three-dimensional variation.

In addition, the vertical velocity structure of the crust-mantle transition may in fact be complex including an actual velocity gradient, which could represent several structural complexities (gradually intruded lower crust, low uppermost mantle velocities, mechanical mixing in the crust-mantle transition zone, etc.). Here, we face the problem of defining and effectively distinguishing between an actual Moho gradient and the HVLC, not least because they may both be characterised by similar overlapping velocity ranges, but also because they may be caused by the same lower crustal/upper mantle lithologies and their alterations. Unless we can clearly distinguish a Moho gradient and the HVLC as two separate structures with visible discontinuities, we regard both features as the same unit.

Considering these challenges in making an unequivocal interpretation of the results, we define the geological interfaces as follows:

- The upper boundary of the crust-mantle transition is defined as the depth where the velocity model exceeds a Vs of 4.25 km/s. The lower boundary of the crust-mantle transition is defined at the depth where the velocity model displays a major reduction in velocity gradient occurring at Vs > 4.4 km/s. The final "Moho discontinuity" used for regional interpretations is defined halfway between these two interfaces, although obviously it is not an actual discontinuity in case of a gradient.

- The upper boundary of the HVLC is defined at the depth where the velocity model exceeds Vs = 4.1 km/s, which represents the Vs corresponding to frequently observed Vp in HVLC. However, being aware of the model uncertainties, a visual interpretation of the model was made allowing us to define the top HVLC as the location where we observe clear velocity changes, which can sometimes occur at velocities as low as Vs = 4.0 km/s. The top HVLC must always be associated with a visible velocity gradient. The HVLC thickness is defined from the upper HVLC interface to the Moho. As a result of this HVLC definition, every station will return a non-null HVLC thickness. Considering the uncertainties and limitations in resolution of the model, we only consider HVLC thicknesses of ≥ 1 km as a robust result, which partly accounts for the vertical resolution of a P-wave at this depth for the used frequency content used (3.2 km corresponds to a half wavelength at 6.5 km/s and 1 Hz). In the final model displayed in the Result section, we therefore subtract 1 km of HVLC thickness and display the remaining thickness (and minimum 0 km) that we consider as robust.
- Our estimated Moho uncertainty (which also translates into the HVLC uncertainty) then consists of two factors: The first is the modelling uncertainty, which is derived from the standard deviations of the model population, defined by the average of depth differences between the Moho depth (top and bottom crust-mantle transition zone) and the respective model standard deviation. The second is the uncertainty based on the fact that the Moho may be an actual gradient, which makes the definition/approximation as a discontinuity geologically uncertain.

Other, shallower interfaces that are not focus of this study were identified according to the following criteria (see Fig. 5): (1) a shallow sedimentary layer is defined as a velocity discontinuity that crosses Vs ~ 2.5 km/s; (2) a deeper sedimentary layer or uppermost crustal layer boundary is defined where a discontinuity crosses Vs ~ 3 km/s; and (3) a mid-crustal discontinuity is defined at the strongest discontinuity between 10 km depth and the top of HVLC/crust mantle transition.

6. Results

6.1. Crustal thickness and Moho depth

The station-by-station Moho depth estimates surrounding the Labrador Sea, Davis Strait and Baffin Bay show values that range between ~32 km and ~ 47 km (Fig. 6, Table 1). Although the dataset is sparse and irregularly distributed over the study area (Fig. 1), some spatial relationships and trends of Moho depth and tectonic boundaries and terranes can be inferred. Overall, the Moho depth estimates from RF inversion in the study area are comparable to previously published data and regional models that are almost entirely based on independent data (Welford and Hall, 2013; Welford et al., 2018; Lebedeva-Ivanova et al., 2019), which is therefore a good first indication that the estimates are geologically meaningful. However, locally we see considerable differences, which demonstrates the importance of the present work in providing reference points for regional compilations and models.

On the West Greenland margin, the regional trend in Moho depth is consistent with the compiled reference model (combination of ArcCrust, Crust1.0 and crustal models from Welford and Hall, 2013; Welford et al., 2018)), although we obtain generally deeper Moho estimates than previously suggested (Fig. 7). The northern stations on the West Greenland margin (TULEG, KULLO, UPNV, NUUG) show Moho depths that are inconsistent with the reference model, but rather resemble the Moho depths further inland along the West Greenland coastline, which implies that thicker crust may reach closer to the coastline than previously interpreted. The 36 km deep Moho at TULEG is similar to estimates by Darbyshire (2003), Dahl-Jensen et al. (2003) and Kumar et al. (2007) with 35–40 km, 37 km and 36 km, respectively. Equally, similar estimates are observed at UPNV (~38 km, this study; ~35 km, Darbyshire, 2003; 38 km, Dahl-Jensen et al., 2003). Only Kumar et al. (2007) estimated a substantially shallower Moho depth of 32 km at station UPNV. The stations in the vicinity of outcrops of the Davis Strait Igneous Province (DSIP) (UMM, GDH, ASIG, ILUG/ILULI) in central West Greenland clearly show thinned crust compared to the surrounding continental areas in West Greenland, which is also seen in ArcCrust. Dahl-Jensen et al. (2003) estimated a Moho depth of 36 km at station GDH, which is the same as our estimate. However, Kumar et al. (2007) again estimated a shallower Moho of 32 km. The boundary between the Nagssugtoqidian Orogen and the North Atlantic Craton was previously imaged by common conversion point stacking of RFs (Dahl-Jensen et al., 2016) and our inversion results are consistent with these results. Both studies suggest a NW-SE thinning of the crust from approximately 45–50 km in the boundary zone between both terranes to 35–40 km in the North Atlantic Craton. Both Dahl-Jensen et al. (2003) and Kumar et al. (2007) estimated a very deep Moho at station SFJ (47 km and 45 km), which is consistent with our estimate at SFJD (~46 km). The other two stations in the North Atlantic Craton (NUUK, PAAG) show consistently shallower Moho of ~37 and 38 km depth, respectively, compared to the other Precambrian domains in West Greenland. At these stations, Dahl-Jensen et al. (2003) estimated 38 km and 42 km deep Moho, and Kumar et al. (2007) estimated 35 and 41 km, respectively. In the Ketilidian Mobile Belt again slightly deeper Moho at ~40 and 44 km is apparent at the stations IVI and NRS which is consistent with the compiled reference model. Dahl-Jensen et al. (2003) previously estimated a Moho depth of 40 km at NRS.

Along the Canadian Northwest Atlantic margin, we observe more significant differences between our RF inversion results, previous RF

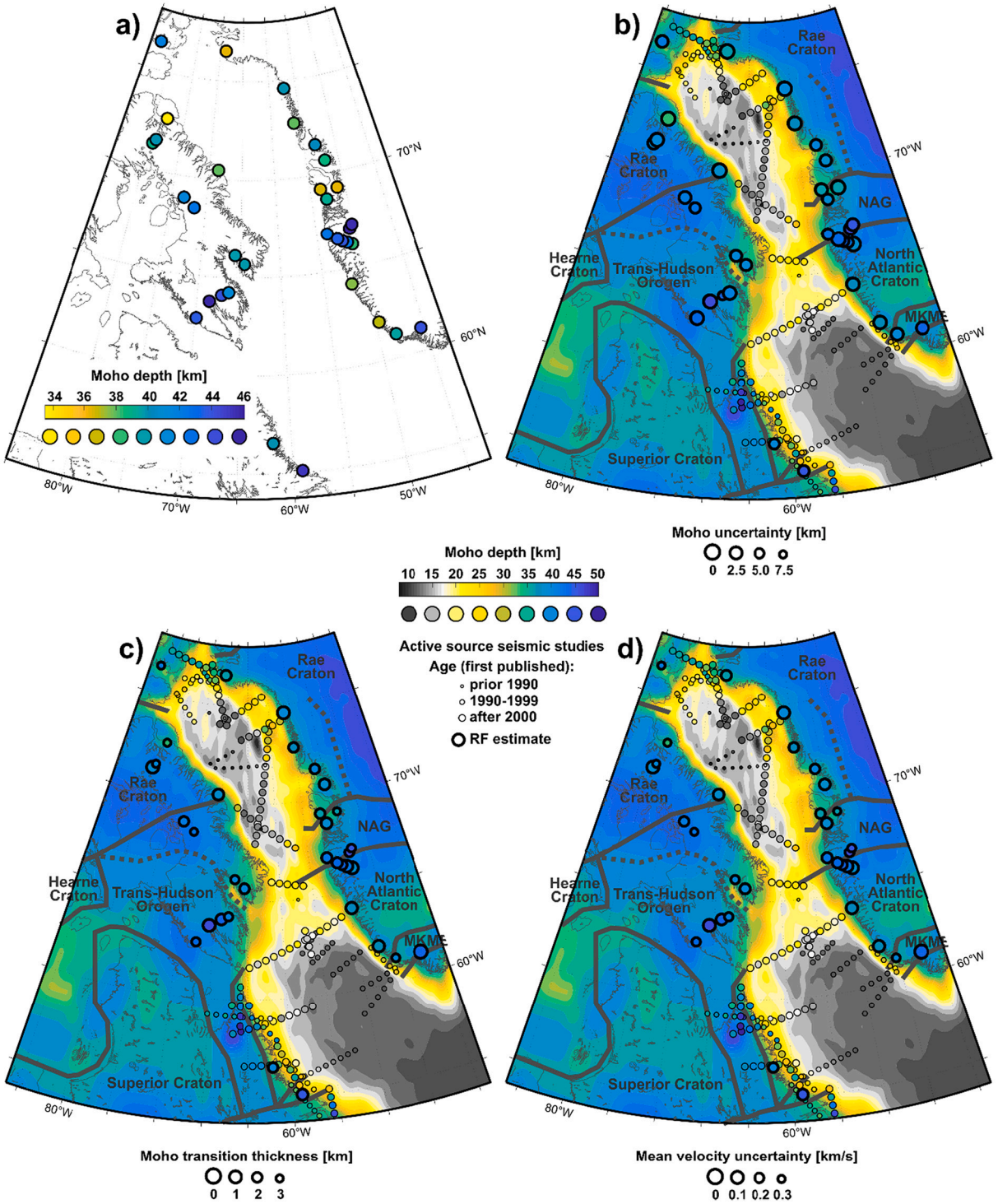

Fig. 6. Moho depth results. (a) shows the inversion result from this study only (colourbar is inserted in map). (b) to (d) show inversion results together with previous published Moho depth estimates (b-d, see Fig. 3 for references) and crustal reference model (Welford and Hall, 2013; Welford et al., 2018; Lebedeva-Ivanova et al., 2019) in the background (colourbar in the centre of figure). Small circles are results from published offshore seismic studies (see Fig. 3 for references). Larger circles with thick black frame are new results from RF inversion. The size of the circles representing RF results is the expression of the uncertainty (large icons representing low uncertainties, small icons representing large uncertainties): b) the estimated model uncertainty (in km); c) the thickness of the crust-mantle transition (in km); d) the mean uncertainty of the velocity model (in km/s). Abbreviations: NAG – Nagssugtoqidian Orogen; MKMB – Makkovik-Ketilidian Mobile Belt.

studies, and the reference model (Fig. 7) (Lebedeva-Ivanova et al., 2019). At the northernmost station used in this study (GFNU), our RF inversion suggests a Moho transition between 40 and 45 km, similar to the maximum Moho depth on southernmost Ellesmere Island and Devon Island according to the reference model, but ~5–7.5 km deeper than estimates by Darbyshire (2003) and ~ 5 km deeper than estimates by Postlethwaite et al. (2014). The next station to the south (POIN/PINU on northernmost Baffin Island) shows a shallow Moho at ~33 km depth, which is similar to the reference model in this area and most previous RF estimates (~35 km, Darbyshire, 2003 and Gilligan et al., 2016; ~34 km, Thompson et al., 2010; 31.5 km, Postlethwaite et al., 2014). Northern Baffin Island (stations CLRN, MRYN, MARC, B1NU and B2NU) is

Table 1
Stations and model estimates (values are colour-coded: white/green – low values, red – large values).

Station	Moho depth [km]	thickness crust-mantle transition [km]	thckness HVLC [km]	Moho uncertainty [km]	average velocity uncertainty [km/s]
ASIG	39.3	1.50	5.00	4.00	0.11
B1NU	42.5	3.00	3.75	4.15	0.20
B2NU	41.5	2.00	2.50	2.69	0.20
CDKN	41.3	2.50	2.50	1.75	0.13
CLRN	45.3	1.00	1.50	1.13	0.13
CMBN	39.9	1.75	5.75	3.29	0.12
FRB	46.0	1.00	2.00	1.50	0.08
GDHO	36.8	2.00	5.50	2.56	0.14
GFNU	42.0	3.00	4.00	2.88	0.20
ILULI/ILUG	36.5	3.00	2.25	1.20	0.10
IVI	39.6	2.75	4.75	2.54	0.17
JENN	44.3	1.50	3.00	6.20	0.20
KIMN	43.8	2.50	3.50	1.70	0.15
KULL	40.0	1.00	2.50	0.94	0.10
MARN	39.0	1.00	3.00	2.92	0.18
MKVL	45.3	1.50	2.50	3.75	0.14
MRYN	40.0	3.00	5.00	1.69	0.11
NANL	40.5	1.00	3.00	4.35	0.14
NRS	44.3	0.50	1.00	2.33	0.15
NUUG	40.5	2.00	4.25	3.63	0.17
NUUK	37.6	1.25	3.25	2.06	0.10
PAAG	37.1	1.25	2.25	1.92	0.15
PNGN	39.8	2.50	5.00	3.44	0.14
POIN	33.5	3.00	3.00	1.25	0.12
SA1G	38.5	1.00	2.00	0.75	0.12
SA2G	42.6	1.25	2.00	4.65	0.16
SA3G	44.0	2.00	4.00	3.85	0.17
SA4G	43.6	1.75	2.75	1.19	0.17
SFJ1	46.1	2.25	3.75	2.66	0.14
SFJ2	45.8	2.50	5.00	2.63	0.17
SISG	42.6	1.75	5.75	3.78	0.10
TULEG	36.4	1.75	1.75	0.96	0.11
UMMO	38.8	1.50	5.50	3.25	0.15
UPNV	38.0	2.00	3.50	1.50	0.13

otherwise characterised by a relatively consistent moderate Moho depth of ~37–43 km, similar to the reference model and previous RF studies (Darbyshire, 2003; Gilligan et al., 2016), with exception of 35 km at station CLRN by Postlethwaite et al. (2014) and up to 44 km at B1NU by Thompson et al. (2010). Stations from southern Baffin Island (CMBN, PNGN, CDKN, FRB, KIMN) show a generally deeper Moho (~40–45 km) than those on northern Baffin Island. Although the differences between north and south are not extreme, it is curious because the reference model suggests the opposite tendency with deeper Moho in the north than in the south. This difference is most pronounced on the Cumberland Peninsula, southeastern Baffin Island (stations CMBN, PNGN), where we observe more than 5 km deeper Moho compared to the reference model and previous RF results (Thompson et al., 2010; Gilligan et al., 2016), with the exception of Postlethwaite et al. (2014), who estimated 33 km at station CMBN. Our Moho estimate at station FRB (45 km) is the same as estimated by Darbyshire (2003) and only slightly deeper than other models (Thompson et al., 2010; Postlethwaite et al., 2014). Stations CDKN and KIMN show similar Moho depth values as previous studies (Thompson et al., 2010; Postlethwaite et al., 2014), with the exception of a larger Moho depth at station KIMN by Postlethwaite et al. (2014). In the Nain province, we observe a 40 km deep Moho at station NANL on the central Labrador coast, approximately 5 km deeper than the reference model, similar to the Moho depth in northern Labrador and further inland (Funck and Louden, 1999; Funck et al., 2000b), but over 10 km deeper than estimated by Postlethwaite et al. (2014). At this location, Vervaet & Darbyshire (2022) estimated a Moho depth of ~35–40 km. However, considerably higher velocities were inferred in the uppermost layers (about 3.0–3.5 km/s compared to 2.6 km/s in this study), which could relate to a velocity pull-down explaining the difference in Moho depth. The estimated Moho depth in the Makkovik province (station MKVL) is 45 km which is similar to that in the Ketilidian Mobile Belt (stations NRS and IVIG) on the West Greenland conjugate margin, and slightly thinner than the ~45–50 km deep Moho estimated by Vervaet & Darbyshire (2022), but again considerably thicker than the estimate of 26 km by Postlethwaite et al. (2014).

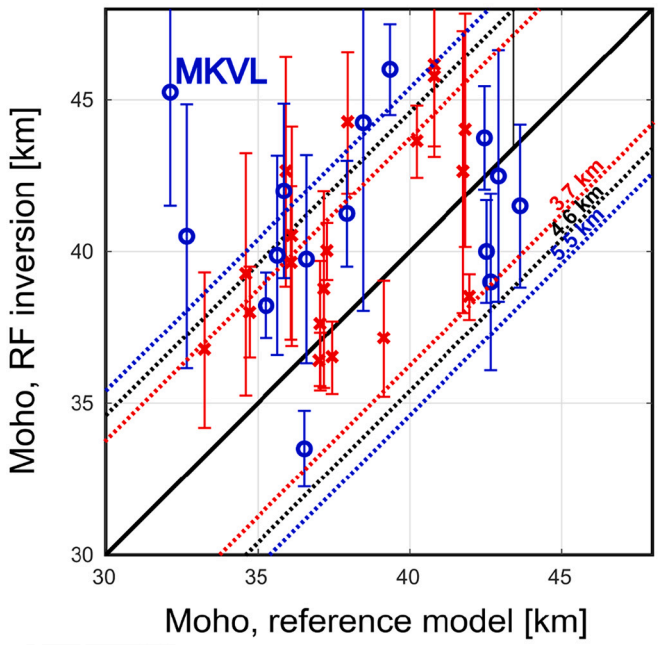

Fig. 7. Comparison of Moho depth of the complied reference model (x-axis) and Moho depth estimated from receiver function inversion in this study (y-axis). Blue dots mark estimates from Northeast Canada, red crosses mark estimates from West Greenland. Error bars are the estimated model errors from inversion. Black line shows a one-to-one correlation between both models. Dotted lines mark the RMS difference between both models (red – West Greenland, black – all estimates, blue – Northeast Canada). It is evident that RF inversion overall estimates deeper Moho than the reference model and that Northeast Canada (blue) has larger mismatches than West Greenland (red). (For interpretation of the references to colour in this figure legend, the reader is referred to the web version of this article.)

The regional Moho depth variation on the Canadian Labrador-Baffin margin compares well with the West Greenland conjugate: Northern Baffin Island and the conjugate West Greenland Rae Craton/Rinkian Orogen show moderate Moho depth; Southern Baffin Island and the conjugate Nagssugtoqidian Orogen have thick crust; The Nain and Makkovik Provinces show very similar results as the conjugate North Atlantic Craton and Ketilidian Mobile Belt, respectively.

These new RF results are important as they add reference points to new regional crustal models and provide a deeper understanding crustal processes and structure, whilst they also support the previously established existence of terrane boundaries and sutures in the region.

6.2. *Thickness of high velocity lower crust (HVLC)*

Our new RF inversion results from the Labrador Sea, Davis Strait and Baffin Bay margins indicate the presence of HVLC below the present-day onshore regions and allow a reinterpretation of the distribution and origin of these structures. As illustrated in previous sections, there are a number of challenges in the interpretation of these results, specifically: (a) interpreting the origin and age of HVLC, and (b) defining the exact vertical extent/thickness of HVLC considering overlapping velocity ranges, Moho gradients and model uncertainty.

The results of the HVLC thickness are shown in Fig. 8, together with the interpretation of the HVLC type and origin, which will be discussed in later sections.

In West Greenland, there are clear indications of HVLC in the Disko Bay area with thicknesses of 4–5 km (stations NUUG, UMM, GDH, ASIG, SISG), with the exception of station ILUG/ILULI where the HVLC thickness is negligible. Moderate thicknesses of 1–3 km were estimated at the stations immediately to the north (stations KULLO and UPNV) and south (stations SA1G–4G, NUUK, PAAG, IVIG) of the Disko Bay area. Only three stations show negligible HVLC thicknesses, and these are the northernmost station (TULEG), the easternmost station in the Disko Bay area (ILUG/ILULI) and the southernmost station (NRS).

On the Canadian side, only two stations on the Cumberland Peninsula (PNGN and CMBN) exhibit thick HVLC of 4–5 km. These are surrounded primarily by stations indicating thin HVLC of 1–2 km, after subtraction of 1 km (CLRN, B2NU, CDKN, JENN, FRB, KIMN), which is close to the detection limit of RFs. The southernmost station in the Makkovik Province (MKVL) also shows a HVLC of only 1-2 km. Moderately thick HVLC (1–3 km) is found in the north (GFNU, POIN/PINU, MRYN/MARN). Station B1NU with a HVLC thickness of 2 km is situated in the vicinity of otherwise thinner HVLC.

7. Discussion

7.1. *Implications for regional crustal models*

We collected teleseismic data from all available seismic stations around the Northwest Atlantic and estimated crustal structure using RF inversion. Our model has the advantage that we are treating all available stations with the same methodology, compared to previous studies that treated various sub-datasets with different methods and processing steps. Most previous RF estimates were based on H-κ stacking, which treats the crust as a single layer and cannot account for crust-mantle transition zones, the presence of HVLC or other intra-crustal complexities – all important complementary information which we focus our interpretations on.

Our new Moho results from West Greenland are generally more consistent with the regional crustal reference models (root mean square difference of 3.7 km) than those from the Canadian margin (root mean

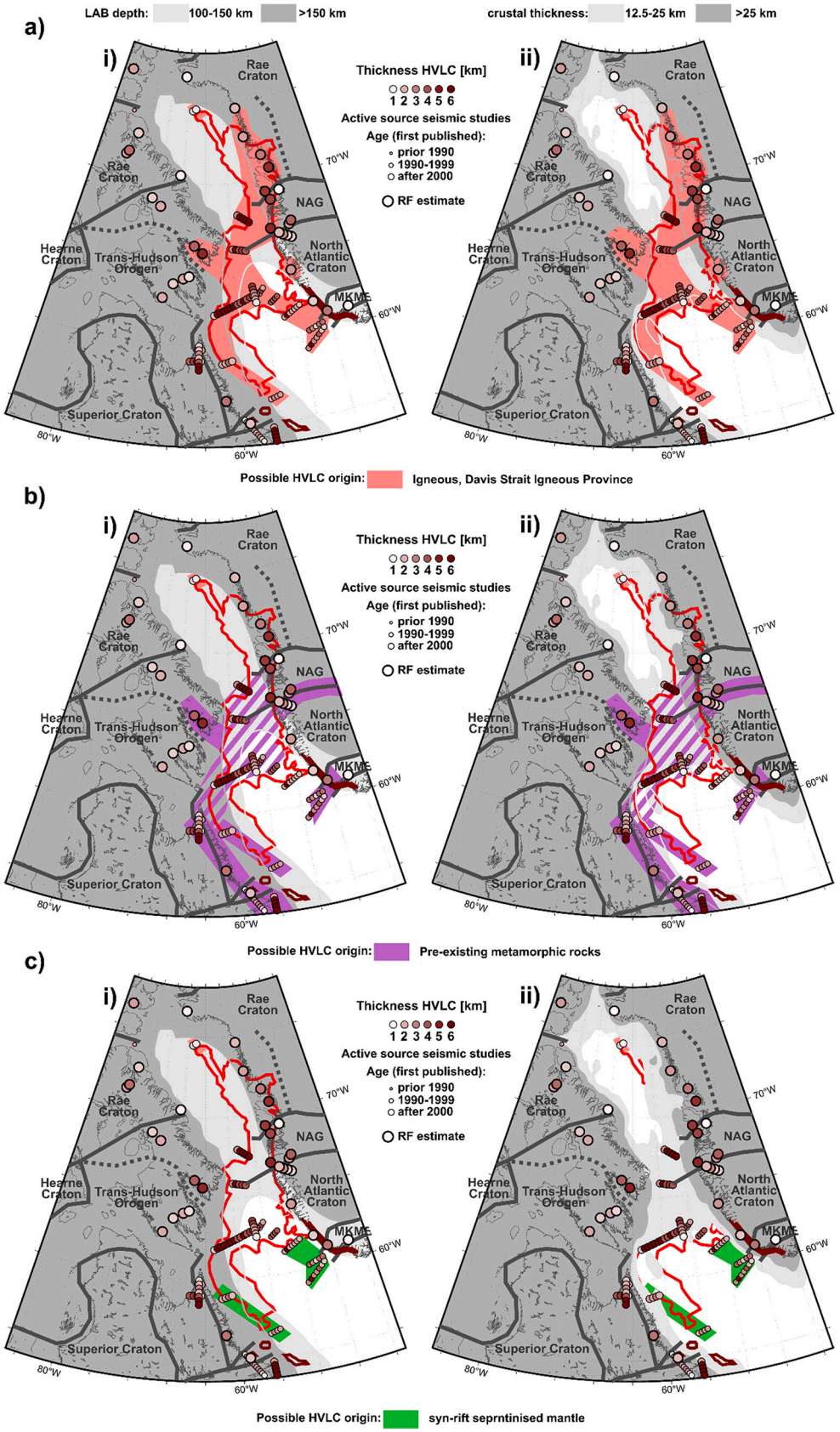

Fig. 8. Estimates and interpretation of the thickness of high velocity lower crust (HVLC) with (i) the Lithosphere-Asthenosphere boundary (LAB) depth, and (ii) crustal thickness in the background. In a), b) and c), the differently shaded areas mark different interpretations of HVLC: red indicates a possible igneous HVLC origin, purple marks interpreted orogenic-type HVLC and green shading marks interpreted exhumed mantle-type HVLC. Stippled areas mark more uncertain areas. Red line marks the outline of previously mapped igneous products of the Davis Strait Igneous Province. NAG – Nagssugtoqidian Orogen; MKMB – Makkovik-Ketilidian Mobile Belt. (For interpretation of the references to colour in this figure legend, the reader is referred to the web version of this article.)

square difference of 5.5 km) (Fig. 7). Of 34 stations at which the Moho depth was estimated, 25 estimates indicate a deeper Moho than the crustal reference model, while only 9 stations indicate a shallower Moho depth, indicating that there is a systematic tendency of the RF inversion (and interpretation of the velocity models) towards a deeper Moho depth than the Moho suggested by the regional reference model.

Across West Greenland, changes in Moho depth appear to be dependent on defined tectonic provinces, as shown in a schematic cross section (Fig. 9a). In the north, the Moho depth is relatively shallow under the Rae Craton, increasing in depth following the transition to the crust of the Rinkian Orogen. The Nagssugtoqidian Orogen generally displays the thickest crust in West Greenland, together with the Disko Bay area, which also shows clear evidence for crustal thinning likely related to magmatism and rifting. The Moho depth increases southwards to the boundary with the North Atlantic Craton, likely related to the amalgamation of Greenland. The remaining crust of the North Atlantic Craton is generally thinner than this orogenic/sutured crust. In the south, the Ketilidian Mobile Belt in southernmost Greenland exhibits thicker crust than the North Atlantic Craton. Finally, the Disko Bay area clearly shows evidence for crustal thinning, likely related to magmatism and rifting, confirming earlier studies.

On the Canadian side (Fig. 9b), we emphasise the following main features: (i) A consistent north-south Moho depth increase on Baffin Island. The Rae Craton has the overall thinnest crust, followed by the northern segment of the Trans-Hudson Orogen on Baffin Island and finally the southern segment of the Trans-Hudson Orogen with clearly thickest crust, which supports the notion of the Baffin Suture dividing Baffin Island. Curiously, this is the opposite trend than what the reference crustal model depicts. (ii) The Central Labrador coast comprises thick crust, which appears to be related to the Torngat Orogen, clearly mapped in the north of Labrador by previous seismic surveys. (iii) The Makkovik province (station MKVL) has a deep Moho, in the same range as the conjugate Ketilidian Mobile Belt. Our Moho depth estimate at MKVL seems to be robust, and recent RF inversion results from a different code and approach suggests a very similar depth (Vervaet & Darbyshire 2022). However, this estimate is ~13 km deeper than the reference model and published controlled source seismic models in the Makkovik Province (Louden and Fan, 1998), which may indicate a complex crust-mantle transition zone.

7.2. Extent and origin of high velocity lower crust

As explained before, knowing which type of HVLC is present in the lower crust can provide key insight into the past geodynamic events that have affected a region, such as igneous activity, mantle serpentinisation and orogeny. In the following section, we will first present an interpretation of our new results combined with results from previous studies, by assigning observed lower-crustal structure to the four main types of possible HVLC; i) igneous, ii) pre-existing metamorphic, iii) *syn*-rift exhumed and serpentinised mantle, and iv) cratonic lower crust type HVLC body. Then we will discuss the distribution of these different types of HVLC across the NW Atlantic (Fig. 10). Our interpretations are guided by surface geology, as limited other information is available, and we recognise that more complex structures may exist and that the mapped geology may be incomplete. The new models of HVLC thickness, in relation to existing data as well as regional geology and tectonics, allow for an improved interpretation of the distribution of HVLC and its origin. This improved interpretation is based on spatial correlation with volcanic provinces, known suture zones and terrane boundaries, or with crustal and lithospheric thickness. All HVLC thickness interpretations and all values mentioned are based on the RF inversion estimates with 1 km subtracted in order to account for uncertainties. HVLC thickness below 1 km is therefore assumed to be negligible/non-existent.

Where HVLC is in the vicinity of, or coincident with, other observations of igneous rocks of the Davis Strait Igneous Province (DSIP), we interpret these structures as a mafic underplate, or lower crustal intrusions related to DSIP magmatism, unless evidence suggests otherwise. Similarly, if HVLC is found in the vicinity or as an extrapolation of known tectonic boundaries or in orogens and mobile belts, we consider the possibility that HVLC represents a fossil metamorphosed crustal root. For example, the HVLC beneath the Davis Strait may partly originate from rifting which led to deformation and redistribution of metamorphosed lower crust, rather than entirely from igneous processes, as often assumed (Funck et al., 2007; Gerlings et al., 2009; Funck et al., 2012; Keen et al., 2012; Hosseinpour et al., 2013; Suckro et al., 2013). In areas where we see thinned crust and HVLC in direct contact with

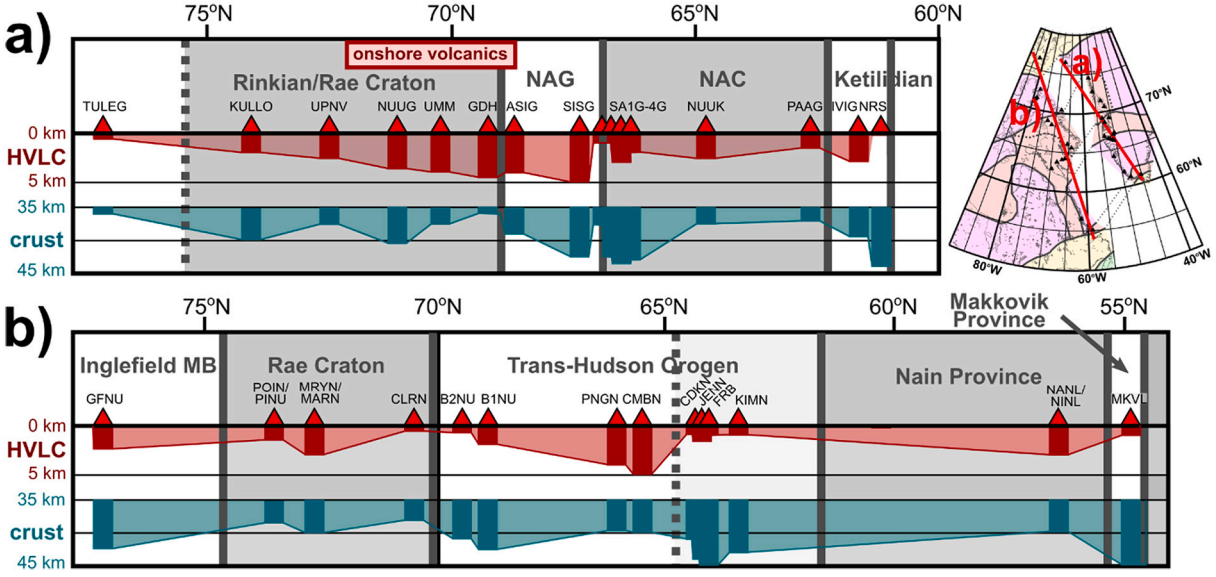

Fig. 9. Thickness of high velocity lower crust (HVLC) and crustal thickness along transects across the West Greenland (a) and East Canada margins (b). The red vertical bars represent the thickness of the HVLC. The green vertical bars represent the crustal column (note that the graph is truncated at 35 km) and the lower end consequently marks the Moho. NAG – Nagssugtoqidian Orogen; NAC – North Alantic Craton. Vertical grey lines roughly indicate projected terrane boundaries and different grey/white shaded areas mark terranes. (For interpretation of the references to colour in this figure legend, the reader is referred to the web version of this article.)

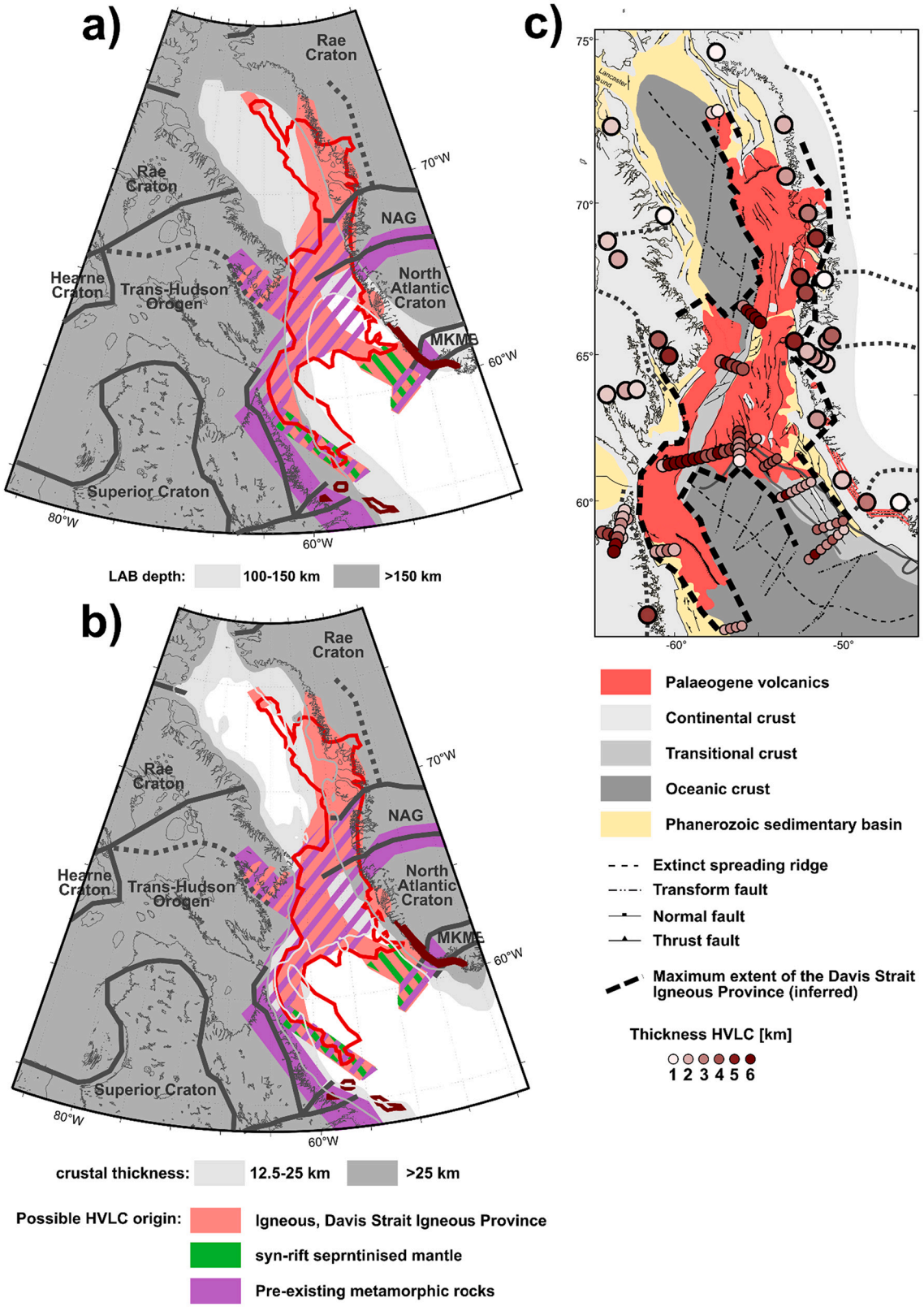

Fig. 10. Estimates and interpretation of the thickness of high velocity lower crust with (a) the Lithosphere-Asthenosphere boundary (LAB) depth, (b) crustal thickness and (c) the simplified geological map in the background. In a) and b) red shaded areas mark interpreted igneous-type HVLC, purple marks interpreted orogenic-type HVLC and green shading marks interpreted exhumed mantle-type HVLC. Stippled areas mark two possible interpretations. Red line marks the outline of previously mapped igneous products of the Davis Strait Igneous Province. The thick black-stippled line in (c) marks the possible extent of the Davis Strait Igneous Province. (For interpretation of the references to colour in this figure legend, the reader is referred to the web version of this article.)

sedimentary successions, HVLC may be indicative of syn-rift exhumed mantle. We also use the distribution of different HVLC bodies and their interpretation in a palaeogeographic reconstruction (Fig. 11) in order to evaluate whether or not HVLC of the same type is spatially related. In addition, the interplay between HVLC and Moho depth is another good indicator for the type of HVLC: lower crustal intrusions may more commonly appear in regions of thinned crust, whilst orogenic-type HVLC rather occurs in thickened crust (but obviously with some exceptions).

In West Greenland, the estimated HVLC in the Disko Bay area corresponds well with mapped occurrences of igneous rocks in the region. A DSIP-origin of the HVLC in this area is supported by the observations between 67°N (station ASIG) and 71°N (Upernavik, station UPNV) (Fig. 9). Whether or not HVLC as far north as 73°N (station KULLO) is related to the DSIP is uncertain as the estimated HVLC thickness is decreasing and no Palaeogene igneous products were mapped on- or offshore (Fig. 2). The potential continuation of the DSIP in this area may be investigated in future studies. On mainland Greenland opposite to Disko Island, the HVLC thickness is negligible (station ILUG/ILULI). We interpret this station to mark the eastern limit of the DSIP in this area. More data are required to map the extent, thickness and structural relationships of HVLC in this area.

To the south, station SISG, the closest to the coastline of 5 stations in a temporary array in central West Greenland (Dahl-Jensen et al., 2016), shows thick HVLC (Figs. 8-10). Although in the onshore there are no reported outcrops of Palaeogene igneous rocks, there is evidence for such rocks in the offshore (Funck et al., 2012; Suckro et al., 2013; Abdelmalak et al., 2019). Therefore, it is possible that the HVLC at SISG is of igneous nature, which would imply that the DSIP has affected the area.

Immediately to the east of SISG, the other 4 temporary stations (SA1G-SA4G) cross the boundary between the Nagssugtoqidian Orogen and North Atlantic Craton (Figs. 8-10). The HVLC estimated here is considerably thinner (2–4 km) than at SISG. A similar thickness (4–5 km) was estimated at station SFJD further east, which is still close to the elusive tectonic boundary. We interpret this HVLC as a possible remnant of the orogenic processes that resulted from the collision of the Nagssugtoqidian Orogen and North Atlantic Craton.

Station NUUK displays a moderately thick HVLC of ~2.5 km. Only minor intrusions are mapped in the area and a sill complex is mapped in the offshore, but there is no evidence for HVLC in the offshore (Funck et al., 2007). Furthermore, station NUUK is at considerable distance to known suture zones or terrane boundaries. We cannot make strong inferences about the origin of this estimated HVLC, and it may be either related to igneous processes, or could represent a cratonic-type lower crustal layer of the North Atlantic Craton.

The stations in South Greenland (PAAG, IVI, NRS) show varying HVLC thicknesses (Figs. 8-10). The HVLC at PAAG, the northernmost of these, is ~2 km thick, followed by a thickness of ~5 km at IVI and negligible thickness at the southernmost station, NRS. None of these stations can be related to Palaeogene igneous rocks, but a Cretaceous dyke swarm follows the coastline in this area (Larsen et al., 2009). Here, the continent-ocean transition is interpreted to be close to the present-day coastline due to a very narrow shelf (Dunbar and Sawyer, 1989; Chian et al., 1995b; Chian et al., 1995a; Chalmers and Pulvertaft, 2001; Peace et al., 2016) and the nature of the offshore HVLC is debated (e.g. Chian et al., 1995b). The distal part of the offshore HVLC is likely in contact with sediments, which could allow transport of water into the mantle during rifting and makes a serpentinised mantle type HVLC a likely candidate. Vice versa, the proximal part of the HVLC underlies continental crust and for the same reasons, a hydrated, serpentinised mantle type HVLC is here rather unlikely. Therefore, the nature of the thick HVLC at PAAG and IVI is uncertain: At PAAG the HVLC could either represent moderate lower crustal intrusions or a cratonic lower

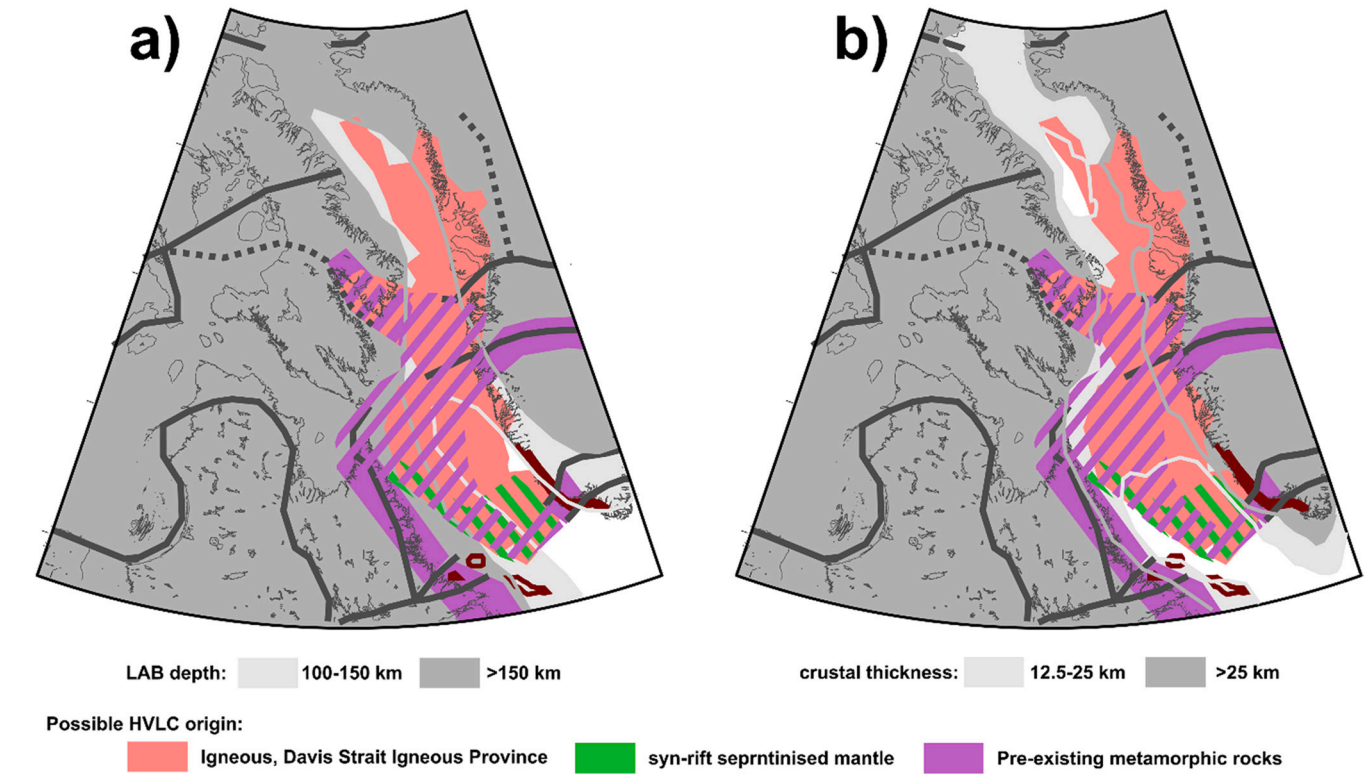

Fig. 11. Reconstructions of the lithosphere-asthenosphere boundary depth (a) and crustal thickness (b) of the NW Atlantic area at 62 Ma (from Abdelmalak et al. 2017) with interpretations of observed high velocity lower crustal (HVLC) bodies. Red shaded areas mark interpreted igneous-type HVLC, purple marks interpreted orogenic-type HVLC and green shading marks interpreted exhumed mantle-type HVLC. Stippled areas mark two possible interpretations. (For interpretation of the references to colour in this figure legend, the reader is referred to the web version of this article.)

crust of the North Atlantic Craton; At IVIG, the HVLC may represent a local igneous alteration of the lower crust, possibly breakup related, or it could be related to the North Atlantic Craton-Ketilidian boundary and thereby collision processes.

On the Canadian side, the only estimates of HVLC from this study that could possibly relate to the DSIP are those on the Cumberland Peninsula (stations PNGN, CMBN). These three stations have an HVLC that is 5–6 km thick, which is noticeably thicker than the estimates at other stations on Baffin Island. However, in this area there is no evidence of Palaeogene igneous rocks or any other magmatism, except for the HVLC of the Davis Strait offshore and outcrops at the easternmost tip of Cumberland Peninsula – both of these locations are at more than 100 km distance to stations PNGN and CMBN. Another process that could explain this thick HVLC is the amalgamation of the Trans-Hudson Orogen. Indeed, an intra-Trans-Hudson Orogen terrane boundary, the Baffin Suture, separates southern and northern Baffin Island (Corrigan et al., 2009; St-Onge et al., 2009) and this boundary is close to stations PNGN and CMBN. The HVLC along this boundary could therefore represent preserved metamorphic rocks related to suturing of Palaeoproterozoic terranes. Nevertheless, interpretation of this HVLC remains speculative and requires more work and supporting data to establish spatial and structural relationships. All other estimates on Baffin and Devon Island show HVLC thicknesses of 2–4 km, generally thicker in the north than in the south and we relate these estimates to a lower crustal layer that can sometimes be observed in cratonic areas (England and Ebbing, 2012; Thybo and Artemieva, 2013; Schulte-Pelkum et al., 2017).

Northern Labrador has been previously shown to be underlain by more than 5 km thick HVLC related to Palaeoproterozoic collision of the Archean Nain Province (Funck and Louden, 1999; Funck et al., 2000b). The thick HVLC at station NANL (central Labrador coast) likely represents the southward continuation of the Palaeoproterozoic Torngat Orogen and similar amalgamation processes between the Nain Province/North Atlantic Craton to the east with Palaeoproterozoic terranes to the west. An igneous interpretation of this HVLC relating to the DSIP is unlikely, due to the lack of Mesozoic-Cenozoic magmatism in the immidiate surroundings.

Only very thin or no HVLC was estimated in the Makkovik province (MKVL), the southernmost station of this study. Peace et al. (2016) have found only little evidence for rift-related magmatism in the Makkovik Province and our estimates are in agreement with a coincident seismic refraction line showing only the presence of a minimal HVLC layer (Louden and Fan, 1998). We prefer an orogenic-type HVLC in this area, related to Grenvillian tectonics (Funck et al., 2001).

Maps showing the distribution of the three major types of HVLC, i.e., 1) igneous/magmatic, 2) orogenic and 3) *syn*-rift exhumed mantle type in relation to LAB and Moho depths are shown on Fig. 8. A final map integrating all the available information and depicting our preferred distribution of HVLC types is shown in Fig. 10, and its reconstruction at 62 Ma in Fig. 11.

Fig. 8a shows the maximum extent of possible igneous-type HVLC. The new data suggest substantial HLVC on the West Greenland margin and on the Cumberland Peninsula on Baffin Island that we regard as candidates for being related to DSIP igneous activity, based primarily on their vicinity to volcanic products onshore and offshore. Furthermore we infer that all HVLC along the Labrador Sea conjugate margins could potentially be of igneous nature (Chian and Louden, 1994; Chian et al., 1995b; Chalmers, 1997), but especially those that are interpreted to be located beneath a layer of intact continental crust in the rifted margin. In such cases, it seems unlikely that water is transported/circulated through the remaining crystalline crust in order to hydrate and serpentinise the uppermost mantle.

Fig. 8b shows the extent of HVLC interpreted here to potentially represent pre-existing metamorphic material in the lower crust. This interpretation is primarily based on the vicinity of these locations to known terrane boundaries and suture zones, such as on the Cumberland Peninsula (Baffin Bay Suture), along the Labrador margin (Torngat Orogen), as well as in the vicinity of the Nagssugtoqidian Orogen-North Atlantic Craton boundary and the Ketilidian Mobile Belt. We furthermore suggest that a substantial part of the HVLC beneath Davis Strait may represent deformed lower (metamorphosed) continental crust of the Nagssugtoqidian Orogen that flowed during the oblique and inheritance-assisted rifting process filling the area forming the Davis Strait, similar to models suggested for the Greenland-Iceland-Faroes Ridge in the Northeast Atlantic (Petersen et al., 2018; Foulger et al., 2020).

Fig. 8c shows the occurrences of HVLC that can potentially be related to syn-rift mantle serpentinisation. However, as noted above, methodological limitations place potential caveats on these interpretations. In cases where the HVLC is in direct contact with sedimentary successions, we interpret a hydrated mantle as a very likely source as opposed to occurrences of HVLC beneath a thinned, but still-intact continental crustal layer.

For all other HVLC bodies for which we cannot find spatial relationships with other geological structures, inferences regarding the origin of HVLC involved too much uncertainty. Many of the occurrences of HVLC in the interior of cratons may be related to a cratonic lower crustal layer that has been observed in numerous regions (e.g. Christensen and Mooney, 1995; England and Ebbing, 2012; Schulte-Pelkum et al., 2017). As already discussed, HVLC can frequently be observed in cratons but they are not ubiquitous. The origin of these bodies is not conclusively understood, but could be related to melt residues, presence of eclogite, or generally crustal formation or modification processes in Archean-Palaeoproterozoic geodynamic settings (Schmidt, 2000; Kukkonen et al., 2008; England and Ebbing, 2012; Schulte-Pelkum et al., 2017).

Our final regional interpretation is presented in Fig. 10. We suggest that the DSIP continues further north on the West Greenland margin than previously mapped. HVLC on the southern West Greenland margin may be part of the DSIP as well, but this interpretation has a higher degree of uncertainty. The lower crust on the Cumberland Peninsula (Baffin Island) may have also been affected by DSIP activity. However, here the close vicinity to the Baffin Suture makes a pre-existing metamorphic origin of this HVLC more likely. The HVLC along the Labrador Sea margins could be explained by several models - igneous injection, metamorphism or syn-rift serpentinisation and based on the available data, we cannot identify a preferred model and suggest a thorough re-investigation and interpretation for future studies. Through our systematic evaluation of possible scenarios, we determined that the most likely one is a metamorphic/orogenic origin for the HVLC mapped along the eastern Labrador coast, in the vicinity of the Nagssugtoqidian Orogen-North Atlantic Craton boundary, as well as in the Ketilidian Mobile Belt.

The relative location of HVLC bodies at 62 Ma using a reconstruction by Abdelmalak et al., (2019) gives further insight into the origin of HVLC (Fig. 11). The potential igneous HVLC now forms a continuous area from northern Baffin Bay to the southern Labrador Sea, except for the bodies on the Cumberland Peninsula, which seem less well-aligned compared to all other HVLC observed. Instead, HVLC on the Cumberland Peninsula may be more likely of orogenic origin, as now the Baffin Suture lines up with the conjugate boundary between Nagssugtoqidian and Rae Craton in West Greenland, forming a lineament of potentially orogenic metamorphosed lower crust. The HVLC potentially formed by syn-rift mantle exhumation and hydration defines a continuous area in the very south of the investigated HVLC bodies, however the HVLC branching out towards the Labrador coast appears to be different and has no corresponding body on the conjugate margin. Furthermore, there is a gap between this offshore HVLC and the HVLC imaged onshore, which may indicate that these are separate bodies. Therefore, it may be more likely that these bodies formed through igneous processes.

An improved distinction between the different types of HVLC will come from future investigations combining coincident, high-resolution datasets from complementary geophysical approaches (gravity,

magnetics, different seismic methods, magnetotellurics, etc.) with detailed structural models.

7.3. Structural and magmatic development of the Northwest Atlantic

The volcanic products of the DSIP are clearly related to the Davis Strait bathymetric high, as well as thickened crust and lithosphere, which suggests a common generic formation process (Fig. 9). Furthermore, we see a clear asymmetry in the distribution of volcanic products (Fig. 9) and coincident sediment-accumulation zones/basins (Fig. 3b), with flipped polarity from north to south (i.e., contrasting volcanism and sedimentary deposition between the eastern Baffin Bay margin and the western Labrador Sea margin). This asymmetry has been noted in other first-order structural aspects of the margins (Peace et al., 2016). The fact that the Davis Strait incorporates a major transfer system, regional control on the distribution of sedimentation and magmatism (Peace et al., 2017; Peace et al., 2018b; Heron et al., 2019; Schiffer et al., 2020), volcanism with ambiguous geochemistry and petrology (Hole, 2015; Clarke and Beutel, 2020; Hole and Natland, 2020) and the simple correlation between extensive igneous products and continental structures all suggest that tectonic processes and inheritance play a major role in the development of the Northwest Atlantic. The magmatic products in Baffin Bay are concentrated on the eastern margin, along the Rinkian Orogen, which may suggest some type of reactivation of Rinkian orogenic structures during breakup of Baffin Bay, as noted by Schiffer et al. (2020). Petersen and Schiffer (2016) have studied the effect of various types of orogenic inheritance on rifting and magnetism and see a clear asymmetry in both margin architecture and magnetic products depending on various pre-existing structural configurations, which could be applied to the Northwest Atlantic. Moreover, Heron et al. (2019) and Clarke and Beutel (2020) have investigated other aspects and other types of structural inheritance that may explain some of these observations in the Northwest Atlantic.

Similar to models developed for the Northeast Atlantic, the structural and magmatic peculiarities could be caused by an oblique interaction of a propagating rift with inherited crustal structures, such as the ancient crustal root of the Nagssugtoqidian Orogen, which also may have caused structural complexity in form of the Greenland-Iceland-Faroes Ridge at a very similar location on the eastern side of Greenland (Foulger et al., 2020; Schiffer et al., 2020).

8. Conclusions

This study presents new crustal velocity models, and therewith estimates of Moho depth and the thickness of HVLC. These two elements provide important new insight into the geodynamic and magmatic evolution in the area. Although a considerable amount of data on the crustal structure exist offshore of the Labrador Sea, Davis Strait and Baffin Bay, deep structural information is limited onshore. The results provide crucial data to map Moho depth and the extent of HVLC, which contribute to updated interpretations of the regional models, as well as interpretations of the extent of the Davis Strait Igneous Province, the presence of fossil collision/subduction zones and sutures/terrane boundaries.

8.1. Extent of the Davis Strait Igneous Province

The new data allow us to infer that the Davis Strait Igneous Province (DSIP) might continue further north than previously thought in West Greenland, where two stations show evidence for HVLC. In addition, there are also some possible indications of DSIP-related HVLC to the south. However, we cannot rule out an alternative HVLC model such as metamorphosed lower crust, especially in South Greenland (Figs. 9 and 10). The cross section along the West Greenland margin clearly indicates maximum HVLC thickness centred in central West Greenland (Disko Bay area) decreasing to the north and south, with some local anomalies that we relate to orogenic processes. On the Canadian side, there might be a possibility that the Cumberland Peninsula was affected by the DSIP given that two stations show thick HVLC, but we prefer an interpretation as an orogenic-type HVLC here, due to the vicinity of the stations to the Baffin Suture. Though these inferences appear significant, more data is clearly required.

8.2. Fossil collision zones and terranes

The new evidence from crustal thickness/Moho depth and HVLC supports the existence of major collision zones/terrane boundaries. We confirm the existence of a suture zone between the Nagssugtoqidian Orogen and North Atlantic Craton, which was already shown by RF common conversion point imaging (Dahl-Jensen et al., 2016), but now we can also relate this boundary to HVLC in addition to a clear Moho step. In SE Baffin Island, we estimated a thick HVLC that likely relates to the Baffin Suture and Trans-Hudson orogenic processes. Furthermore, we see evidence for a continuation of the thick HVLC keel along the Labrador margin that is interpreted to be the remnant of a metamorphosed lower crustal body originating from the Torngat Orogen (Funck and Louden, 1999). Lastly, the thick HVLC mapped in the Ketilidian Province of South Greenland may relate to similar collisional processes, while we consider a relationship to the DSIP as rather unlikely. Although much of the HVLC mapped offshore by previous seismic studies suggests an igneous origin, we note that substantial volumes of HVLC beneath Davis Strait may be of inherited, orogenic type (Gernigon et al., 2004; Petersen and Schiffer, 2016; Schiffer et al., 2016a), such that the igneous volume might be smaller in these areas than previously thought.

The schematic cross-sections shown in Fig. 9 clearly show changes both in Moho depth and HVLC thickness across or along boundaries between terranes and provinces: The Rae Craton consistently has relatively shallow Moho (35–40 km, with exception of station CLRN); The Trans-Hudson Orogen and Nagssugtoqidian Orogen have deeper Moho (~39–45 km); The North Atlantic Craton and Nain Province have a Moho depth of ~30–35 km (with exception of stations located close to the Nagssugtoqidian Orogen -North Atlantic Craton boundary); the Makkovik-Ketilidian Mobile Belt shows deeper Moho (~40–45 km).

The new RF inversion results on the crustal structure in the Northwest Atlantic region add new reference points for the future development of regional models, for comparisons with other studies and for estimates of the extent and magmatic volumes of the DSIP. As the new models only give point-wise information at 34 stations, the interpretations are clearly spatially and structurally limited. More work is therefore required to confirm our inferences and most importantly, more and denser data coverage along the Labrador-Baffin passive margins will help tying structural relationships from Canada to Greenland and along the margins. The correlation of magmatic products, HVLC and known pre-existing structures and terranes boundaries in the region supports a model in which inheritance plays a major role in localising extension, breakup and magmatism in the Northwest Atlantic. However, whether a thermal mantle upwelling was present or whether the region even required assistance cannot be determined.

We would like to emphasise four regions that could yield particularly useful results from more extensive work: i) better coverage of the Disko Bay region, in particular along the mainland, to trace the potential eastern boundary of the DSIP; ii) the area around station NUUK, which shows evidence for a substantial HVLC thickness, but it is unclear whether it is related to the DSIP. Moreover, greater coverage could give insights into the spatial distribution and origin of the HVLC in this area;

iii) SE and central Baffin Island, to investigate the extent of the HVLC and to distinguish whether the HVLC is of orogenic-type or igneous-type; and finally, iv) More work along the Labrador coast in order to fill the gaps between controlled-source and natural-source seismic constraints and get insight into the distribution and origin of HVLC there.

Example linearised LSQ inversion of station TULEG with 5 (d), 12 (e) and 18 (f) layers.

Credit authors

CS was lead author, developed the inverse approach and produced results and figs.

AP contributed to the interpretation of the results and to the development of the manuscript, with focus on the introductory, geological background, result and discussion sections.

SJ contributed to the interpretation of the results and to the development of the manuscript, with focus on the introductory, geological background, result and discussion sections.

SR was involved in the development of the inverse approach, contributed receiver function data and developed the manuscript with focus on the methodological sections and interpretation.

All authors were involved in developing the submitted version of the manuscript.

Declaration of Competing Interest

The authors declare that they have no known competing financial interests or personal relationships that could have appeared to influence the work reported in this paper.

Acknowledgements

CS is funded by the Swedish Research Council (Vetenskapsrådet, 2019-04843). SJ acknowledges funding from NSERC Discovery Grant RGPIN-2018-03932. Global Lithospheric Imaging with Earthquake Recordings (GLImER) was funded by a Marie Skłodowska Curie—Career Integration Grant 321871 from the European Commission FP7 Programme to SR. AP acknowledges NSERC Discovery Grant RGPIN-2021-04011 for support of his research program. Data were extracted from IRIS Breqfast (https://ds.iris.edu/ds/nodes/dmc/forms/breqfast-request/), EIDA Orfeus (http://www.orfeus-eu.org/data/eida/) and the Canadian National Data Centre (https://www.earthquakescanada.nrcan.gc.ca/stndon/CNDC/index-en.php). Thanks to Fiona Darbyshire for discussions and help with accessing waveform data of Canadian stations. Thanks to Mansour Abdelmalak for sharing the vector image of the Tectonic map of the Davis Strait Igneous Province. We thank three anonymous reviewers for critical and constructive reviews that have contributed to the development of this manuscript.

Appendix A. Supplementary data

Supplementary data to this article can be found online at https://doi.org/10.1016/j.tecto.2022.229235.

References

Abdelmalak, M.M., Faleide, J.I., Planke, S., Gernigon, L., Zastrozhnov, D., Shephard, G. E., Myklebust, R., 2017. The T-reflection and the deep crustal structure of the Vøring Margin, offshore mid-Norway. Tectonics 36 (11), 2497–2523.

Abdelmalak, M.M., Planke, S., Polteau, S., Hartz, E.H., Faleide, J.I., Tegner, C., Jerram, D.A., Millett, J.M., Myklebust, R., 2019. Breakup volcanism and plate tectonics in the NW Atlantic. Tectonophysics 760, 267–296.

Ady, B.E., Whittaker, R.C., 2018. Examining the influence of tectonic inheritance on the evolution of the North Atlantic using a palinspastic deformable plate reconstruction. Geol. Soc. Lond. Spec. Publ. 470, SP470-9.

Altenbernd, T., Jokat, W., Heyde, I., Damm, V., 2014. A crustal model for northern Melville Bay, Baffin Bay. J. Geophys. Res. Solid Earth 119, 8610–8632.

Altenbernd, T., Jokat, W., Heyde, I., Damm, V., 2015. Geophysical evidence for the extent of crustal types and the type of margin along a profile in the northeastern Baffin Bay. J. Geophys. Res. Solid Earth 120. https://doi.org/10.1002/2015JB012307, 2015JB012307.

Altenbernd, T., Jokat, W., Heyde, I., Damm, V., 2016. Insights into the crustal structure of the transition between Nares Strait and Baffin Bay. Tectonophysics 691, 31–47.

Ammon, C.J., 1991. The isolation of receiver effects from teleseismic P waveforms. Bull. Seismol. Soc. Am. 81, 2504–2510.

Ammon, C.J., Randall, G.E., Zandt, G., 1990. On the nonuniqueness of receiver function inversions. J. Geophys. Res. Solid Earth 95, 15303–15318. https://doi.org/10.1029/JB095iB10p15303.

Bastow, I.D., Eaton, D.W., Kendall, J.-M., Helffrich, G., Snyder, D.B., Thompson, D.A., Wookey, J., Darbyshire, F.A., Pawlak, A.E., 2015. The Hudson Bay Lithospheric Experiment (HuBLE): insights into Precambrian plate tectonics and the development of mantle keels. Geol. Soc. Lond. Spec. Publ. 389, 41–67. https://doi.org/10.1144/SP389.7.

Bostock, M.G., 1999. Seismic waves converted from velocity gradient anomalies in the Earth's upper mantle. Geophys. J. Int. 138, 747–756.

Cassidy, J.F., Ellis, R.M., 1993. S wave velocity structure of the northern cascadia subduction zone. J. Geophys. Res. Solid Earth 98, 4407–4421. https://doi.org/10.1029/92JB02696.

Chalmers, J.A., 1997. The continental margin off southern Greenland: Along-strike transition from an amagmatic to a volcanic margin. J. Geol. Soc. 154, 571–576. https://doi.org/10.1144/gsjgs.154.3.0571.

Chalmers, J.A., Laursen, K.H., 1995. Labrador Sea: the extent of continental and oceanic crust and the timing of the onset of seafloor spreading. Mar. Pet. Geol. 12, 205–217. https://doi.org/10.1016/0264-8172(95)92840-S.

Chalmers, J.A., Pulvertaft, T.C.R., 2001. Development of the continental margins of the Labrador Sea: a review. Geol. Soc. Lond. Spec. Publ. 187, 77–105. https://doi.org/10.1144/GSL.SP.2001.187.01.05.

Chalmers, J.A., Larsen, L.M., Pedersen, A.K., 1995. Widespread Palaeocene volcanism around the northern North Atlantic and Labrador Sea: evidence for a large, hot, early plume head. J. Geol. Soc. 152, 965–969.

Chian, D., Louden, K., 1992. The structure of Archean–Ketilidian crust along the continental shelf of southwestern Greenland from a seismic refraction profile. Can. J. Earth Sci. 29, 301–313.

Chian, D., Louden, K.E., 1994. The continent-ocean crustal transition across the Southwest Greenland margin. J. Geophys. Res. Solid Earth 99, 9117–9135.

Chian, D., Keen, C., Reid, I., Louden, K.E., 1995a. Evolution of nonvolcanic rifted margins: New results from the conjugate margins of the Labrador Sea. Geology 23, 589–592. https://doi.org/10.1130/0091-7613(1995)023<0589:EONRMN>2.3.CO;2.

Chian, D., Louden, K.E., Reid, I., 1995b. Crustal structure of the Labrador Sea conjugate margin and implications for the formation of nonvolcanic continental margins. J. Geophys. Res. 100, 24,239-24,253.

Chian, D., Marillier, F., Hall, J., Quinlan, G., 1998. An improved velocity model for the crust and upper mantle along the central mobile belt of the Newfoundland Appalachian orogen and its offshore extension. Can. J. Earth Sci. 35, 1238–1251.

Chong, J., Chu, R., Ni, S., Meng, Q., Guo, A., 2018. Receiver function HV ratio: a new measurement for reducing non-uniqueness of receiver function waveform inversion. Geophys. J. Int. 212, 1475–1485. https://doi.org/10.1093/gji/ggx464.

Christensen, N.I., 1996. Poisson's ratio and crustal seismology. J. Geophys. Res. Solid Earth 101, 3139–3156. https://doi.org/10.1029/95JB03446.

Christensen, N.I., Mooney, W.D., 1995. Seismic velocity structure and composition of the continental crust: a global view. J. Geophys. Res. Solid Earth 100, 9761–9788. https://doi.org/10.1029/95JB00259.

Clarke, D.B., Beutel, E.K., 2020. Davis Strait Paleocene picrites: Products of a plume or plates? Earth-Sci. Rev. 206, 102770 https://doi.org/10.1016/j.earscirev.2019.01.012.

Clayton, R.W., Wiggins, R.A., 1976. Source shape estimation and deconvolution of teleseismic bodywaves. Geophys. J. R. Astron. Soc. 47, 151–177. https://doi.org/10.1111/j.1365-246X.1976.tb01267.x.

Corrigan, D., Pehrsson, S., Wodicka, N., de Kemp, E., 2009. The Palaeoproterozoic Trans-Hudson Orogen: a prototype of modern accretionary processes. Geol. Soc. Lond. Spec. Publ. 327, 457–479. https://doi.org/10.1144/SP327.19.

Corrigan, D., van Rooyen, D., Wodicka, N., 2021. Indenter tectonics in the Canadian Shield: a case study for Paleoproterozoic lower crust exhumation, orocline development, and lateral extrusion. Precambrian Res. 355, 106083 https://doi.org/10.1016/j.precamres.2020.106083.

Courtillot, V., Jaupart, C., Manighetti, I., Tapponnier, P., Besse, J., 1999. On causal links between flood basalts and continental breakup. Earth Planet. Sci. Lett. 166, 177–195. https://doi.org/10.1016/S0012-821X(98)00282-9.

Dahl-Jensen, T., Larsen, T.B., Woelbern, I., Bach, T., Hanka, W., Kind, R., Gregersen, S., Mosegaard, K., Voss, P., Gudmundsson, O., 2003. Depth to Moho in Greenland: receiver-function analysis suggests two Proterozoic blocks in Greenland. Earth Planet. Sci. Lett. 205, 379–393. https://doi.org/10.1016/S0012-821X(02)01080-4.

Dahl-Jensen, T., Voss, P.H., Larsen, T.B., 2016. Crustal structure over the Nagssugtoqidian deformation front in West Greenland: Receiver Function analysis. Geol. Surv. Den. Greenl. Bull. 79–82.

Dalhoff, F., Larsen, L.M., Ineson, J.R., Stouge, S., Bojesen-Koefoed, J.A., Lassen, S., Kuijpers, A., Rasmussen, J.A., Nøhr-Hansen, H., 2006. Continental crust in the Davis Strait: new evidence from seabed sampling. Geol. Surv. Den. Greenl. GEUS Bull. 10, 33–36.

Dam, G., Larsen, M., Sønderholm, M., 1998. Sedimentary response to mantle plumes: Implications from Paleocene onshore successions, West and East Greenland. Geology 26, 207–210.

Darbyshire, F.A., 2003. Crustal structure across the Canadian High Arctic region from teleseismic receiver function analysis. Geophys. J. Int. 152, 372–391. https://doi.org/10.1046/j.1365-246X.2003.01840.x.
Darbyshire, F.A., 2005. Upper mantle structure of Arctic Canada from Rayleigh wave dispersion. Tectonophysics 405, 1–23. https://doi.org/10.1016/j.tecto.2005.02.013.
Darbyshire, F.A., Dahl-Jensen, T., Larsen, T.B., Voss, P.H., Joyal, G., 2017. Crust and uppermost-mantle structure of Greenland and the Northwest Atlantic from Rayleigh wave group velocity tomography. Geophys. J. Int. 212, 1546–1569.
Dickin, A., 2021. Comment on Hinchey (2021): "Lithogeochemical and Nd isotopic constraints on felsic magmatism in the Makkovik Orogen, Labrador, Canada: Implications for assembly of the supercontinent Nuna,". Lithos 392–393, 106093. https://doi.org/10.1016/j.lithos.2021.106093.
Dunbar, J.A., Sawyer, D.S., 1989. Patterns of continental extension along the conjugate margins of the central and North Atlantic Oceans and Labrador Sea. Tectonics 8, 1059–1077.
England, R.W., Ebbing, J., 2012. Crustal structure of Central Norway and Sweden from integrated modelling of teleseismic receiver functions and the gravity anomaly. Geophys. J. Int. 191, 1–11. https://doi.org/10.1111/j.1365-246X.2012.05607.x.
Engström, J., Klint, K.E.S., 2014. Continental collision structures and post-orogenic geological history of the Kangerlussuaq area in the southern part of the Nagssugtoqidian Orogen, central West Greenland. Geosciences 4, 316–334.
Foulger, G.R., Doré, T., Emeleus, C.H., Franke, D., Geoffroy, L., Gernigon, L., Hey, R., Holdsworth, R.E., Hole, M., Höskuldsson, Á., Julian, B., Kusznir, N., Martinez, F., McCaffrey, K.J.W., et al., 2020. The Iceland Microcontinent and a continental Greenland-Iceland-Faroe Ridge. Earth-Sci. Rev. 206, 102926 https://doi.org/10.1016/j.earscirev.2019.102926.
Funck, T., Louden, K.E., 1998. Wide-angle seismic imaging of pristine Archean crust in the Nain Province, Labrador. Can. J. Earth Sci. 35, 672–685.
Funck, T., Louden, K.E., 1999. Wide-angle seismic transect across the Torngat Orogen, northern Labrador: evidence for a Proterozoic crustal root. J. Geophys. Res. Solid Earth 104, 7463–7480.
Funck, T., Louden, K.E., Reid, I.D., 2000a. Wide-angle seismic imaging of a Mesoproterozoic anorthosite complex: the Nain Plutonic Suite in Labrador, Canada. J. Geophys. Res. Solid Earth 105, 25693–25707.
Funck, T., Louden, K.E., Wardle, R.J., Hall, J., Hobro, J.W., Salisbury, M.H., Muzzatti, A.M., 2000b. Three-dimensional structure of the Torngat Orogen (NE Canada) from active seismic tomography. J. Geophys. Res. Solid Earth 105, 23403–23420.
Funck, T., Louden, K.E., Reid, I.D., 2001. Crustal structure of the Grenville Province in southeastern Labrador from refraction seismic data: evidence for a high-velocity lower crustal wedge. Can. J. Earth Sci. 38, 1463–1478. https://doi.org/10.1139/cjes-38-10-1463.
Funck, T., Jackson, H.R., Dehler, S.A., Reid, I.D., 2006. A refraction seismic transect from Greenland to Ellesmere Island, Canada: the crustal structure in southern Nares Strait. Polarforschung 74, 97–112.
Funck, T., Jackson, H.R., Louden, K.E., Klingelhöfer, F., 2007. Seismic study of the transform-rifted margin in Davis Strait between Baffin Island (Canada) and Greenland: what happens when a plume meets a transform. J. Geophys. Res. Solid Earth 112, B04402. https://doi.org/10.1029/2006JB004308.
Funck, T., Hansen, A.K., Reid, I.D., Louden, K.E., 2008. The crustal structure of the southern Nain and Makkovik provinces of Labrador derived from refraction seismic data. Can. J. Earth Sci. 45, 465–481.
Funck, T., Gohl, K., Damm, V., Heyde, I., 2012. Tectonic evolution of southern Baffin Bay and Davis Strait: results from a seismic refraction transect between Canada and Greenland. J. Geophys. Res. Solid Earth 117. https://doi.org/10.1029/2011JB009110.
Garde, A.A., Hamilton, M.A., Chadwick, B., Grocott, J., McCaffrey, K.J., 2002. The Ketilidian orogen of South Greenland: geochronology, tectonics, magmatism, and fore-arc accretion during Palaeoproterozoic oblique convergence. Can. J. Earth Sci. 39, 765–793.
Geoffroy, L., Callot, J.-P., Scaillet, S., Skuce, A., Gélard, J.P., Ravilly, M., Angelier, J., Bonin, B., Cayet, C., Perrot, K., 2001. Southeast Baffin volcanic margin and the North American-Greenland plate separation. Tectonics 20, 566–584.
Gerlings, J., Funck, T., Jackson, H.R., Louden, K.E., Klingelhöfer, F., 2009. Seismic evidence for plume-derived volcanism during formation of the continental margin in southern Davis Strait and northern Labrador Sea. Geophys. J. Int. 176, 980–994. https://doi.org/10.1111/j.1365-246X.2008.04021.x.
Gernigon, L., Ringenbach, J.-C., Planke, S., Le Gall, B., 2004. Deep structures and breakup along volcanic rifted margins: insights from integrated studies along the outer Vøring Basin (Norway). Mar. Pet. Geol. 21, 363–372. https://doi.org/10.1016/j.marpetgeo.2004.01.005.
Gilligan, A., Bastow, I.D., Darbyshire, F.A., 2016. Seismological structure of the 1.8 Ga Trans-Hudson Orogen of North America. Geochem. Geophys. Geosyst. 17, 2421–2433. https://doi.org/10.1002/2016GC006419.
Graham, D.W., Larsen, L.M., Hanan, B.B., Storey, M., Pedersen, A.K., Lupton, J.E., 1998. Helium isotope composition of the early Iceland mantle plume inferred from the Tertiary picrites of West Greenland. Earth Planet. Sci. Lett. 160, 241–255.
Grocott, J., McCaffrey, K.J., 2017. Basin evolution and destruction in an early Proterozoic continental margin: the Rinkian fold–thrust belt of central West Greenland. J. Geol. Soc. 174, 453–467.
Hall, J., Louden, K.E., Funck, T., Deemer, S., 2002. Geophysical characteristics of the continental crust along the Lithoprobe Eastern Canadian Shield Onshore–Offshore Transect (ECSOOT): a review. Can. J. Earth Sci. 39, 569–587. https://doi.org/10.1139/e02-005.
Hannemann, K., Krüger, F., Dahm, T., Lange, D., 2016. Oceanic lithospheric S-wave velocities from the analysis of P-wave polarization at the ocean floor. Geophys. J. Int. 207, 1796–1817. https://doi.org/10.1093/gji/ggw342.
Harrison, J.C., Brent, T.A., Oakey, G.N., 2011. Chapter 40 Baffin Fan and its inverted rift system of Arctic eastern Canada: stratigraphy, tectonics and petroleum resource potential. Geol. Soc. Lond. Mem. 35, 595–626. https://doi.org/10.1144/M35.40.
Heron, P.J., Pysklywec, R.N., Stephenson, R., 2015. Intraplate orogenesis within accreted and scarred lithosphere: example of the Eurekan Orogeny, Ellesmere Island. Tectonophysics 664, 202–213. https://doi.org/10.1016/j.tecto.2015.09.011.
Heron, P.J., Peace, A.L., McCaffrey, K.J., Welford, J.K., Wilson, R., van Hunen, J., Pysklywec, R.N., 2019. Segmentation of rifts through structural inheritance: creation of the Davis Strait. Tectonics 38, 2411–2430.
Hinchey, A.M., 2021. Lithogeochemical and Nd isotopic constraints on felsic magmatism in the Makkovik Orogen, Labrador, Canada: Implications for assembly of the supercontinent Nuna. Lithos 382, 105917.
Hole, M.J., 2015. The generation of continental flood basalts by decompression melting of internally heated mantle. Geology 43, 311–314.
Hole, M.J., Natland, J.H., 2020. Magmatism in the North Atlantic Igneous Province; mantle temperatures, rifting and geodynamics. Earth-Sci. Rev. 206, 102794 https://doi.org/10.1016/j.earscirev.2019.02.011.
Hosseinpour, M., Müller, R.D., Williams, S.E., Whittaker, J.M., 2013. Full-fit reconstruction of the Labrador Sea and Baffin Bay. Solid Earth 4, 461–479. https://doi.org/10.5194/se-4-461-2013.
Jackson, H.R., Reid, I., 1994. Crustal thickness variations between the Greenland and Ellesmere Island margins determined from seismic refraction. Can. J. Earth Sci. 31, 1407–1418. https://doi.org/10.1139/e94-124.
Jackson, H.R., Keen, C.E., Falconer, R.K.H., Appleton, K.P., 1979. New geophysical evidence for sea-floor spreading in central Baffin Bay. Can. J. Earth Sci. 16, 2122–2135.
Jacobsen, B.H., Svenningsen, L., 2008. Enhanced uniqueness and linearity of receiver function inversion. Bull. Seismol. Soc. Am. 98, 1756–1767. https://doi.org/10.1785/0120070180.
Jess, S., Peace, A.L., Schiffer, C., 2020. Sediment supply on the West Greenland passive margin: redirection of a large pre-glacial drainage system. Journal of the Geological Society 177 (6), 1149–1160.
Julià, J., Ammon, C.J., Herrmann, R.B., Correig, A.M., 2000. Joint inversion of receiver function and surface wave dispersion observations. Geophys. J. Int. 143, 99–112. https://doi.org/10.1046/j.1365-246x.2000.00217.x.
Keen, C.E., Barrett, D.L., 1972. Seismic refraction studies in Baffin Bay: an example of a developing ocean basin. Geophys. J. Int. 30, 253–271.
Keen, C.E., Dickie, K., Dehler, S.A., 2012. The volcanic margins of the northern Labrador Sea: Insights to the rifting process. Tectonics 31. https://doi.org/10.1029/2011TC002985.
Keen, C.E., Dickie, K., Dafoe, L.T., 2018. Structural evolution of the rifted margin off northern Labrador: the role of hyperextension and magmatism. Tectonics 37, 1955–1972.
Kennett, B.L.N., 1983. Seismic Wave Propagation in Stratified Media. Cambridge University Press, Cambridge; New York.
Kerr, A., Ryan, B., Gower, C.F., Wardle, R.J., 1996. The Makkovik Province: extension of the Ketilidian mobile belt in mainland North America. Geol. Soc. Lond. Spec. Publ. 112, 155–177.
Kerr, A., Hall, J., Wardle, R.J., Gower, C.F., Ryan, B., 1997. New reflections on the structure and evolution of the Makkovikian-Ketilidian Orogen in Labrador and southern Greenland. Tectonics 16, 942–965.
Kind, R., Kosarev, G.L., Petersen, N.V., 1995. Receiver functions at the stations of the German Regional Seismic Network (GRSN). Geophys. J. Int. 121, 191–202. https://doi.org/10.1111/j.1365-246X.1995.tb03520.x.
King, A.F., McMillan, N.J., 1975. A Mid-Mesozoic breccia from the coast of Labrador. Can. J. Earth Sci. 12, 44–51.
Kiselev, S., Vinnik, L., Oreshin, S., Gupta, S., Rai, S.S., Singh, A., Kumar, M.R., Mohan, G., 2008. Lithosphere of the Dharwar craton by joint inversion of P and S receiver functions. Geophys. J. Int. 173, 1106–1118. https://doi.org/10.1111/j.1365-246X.2008.03777.x.
Kolb, J., 2014. Structure of the Palaeoproterozoic Nagssugtoqidian Orogen, South-East Greenland: Model for the tectonic evolution. Precambrian Res. 255, 809–822. https://doi.org/10.1016/j.precamres.2013.12.015.
Kukkonen, I.T., Kuusisto, M., Lehtonen, M., Peltonen, P., 2008. Delamination of eclogitized lower crust: Control on the crust–mantle boundary in the central Fennoscandian shield. Tectonophysics 457, 111–127. https://doi.org/10.1016/j.tecto.2008.04.029.
Kumar, P., Kind, R., Priestley, K., Dahl-Jensen, T., 2007. Crustal structure of Iceland and Greenland from receiver function studies. J. Geophys. Res. Solid Earth 112, n/a-n/a. https://doi.org/10.1029/2005JB003991.
LaFlamme, C., Sylvester, P.J., Hinchey, A.M., Davis, W.J., 2013. U-Pb age and Hf-isotope geochemistry of zircon from felsic volcanic rocks of the Paleoproterozoic Aillik Group, Makkovik Province, Labrador. Precambrian Res. 224, 129–142. https://doi.org/10.1016/j.precamres.2012.09.005.
Langston, C.A., 1979. Structure under Mount Rainier, Washington, inferred from teleseismic body waves. J. Geophys. Res. Solid Earth 84, 4749–4762. https://doi.org/10.1029/JB084iB09p04749.
Larsen, L.M., Heaman, L.M., Creaser, R.A., Duncan, R.A., Frei, R., Hutchison, M., 2009. Tectonomagmatic events during stretching and basin formation in the Labrador Sea and the Davis Strait: evidence from age and composition of Mesozoic to Palaeogene dyke swarms in West Greenland. J. Geol. Soc. 166, 999–1012.
Larsen, L.M., Pedersen, A.K., Tegner, C., Duncan, R.A., Hald, N., Larsen, J.G., 2016. Age of Tertiary volcanic rocks on the West Greenland continental margin: volcanic evolution and event correlation to other parts of the North Atlantic Igneous Province. Geol. Mag. 153, 487–511.

Laske, G., Masters, G., Ma, Z., Pasyanos, M., 2013. Update on CRUST1. 0—A 1-degree global model of Earth's crust. In: Geophys. Res. Abstr, EGU General Assembly Vienna, Austria, p. 2658.
Lebedev, S., Schaeffer, A.J., Fullea, J., Pease, V., 2018. Seismic tomography of the Arctic region: inferences for the thermal structure and evolution of the lithosphere. Geol. Soc. Lond. Spec. Publ. 460, 419–440.
Lebedeva-Ivanova, N., Gaina, C., Minakov, A., Kashubin, S., 2019. ArcCRUST: Arctic crustal thickness from 3-D gravity inversion. Geochem. Geophys. Geosyst. 20, 3225–3247.
Louden, K.E., Fan, J., 1998. Crustal structures of Grenville, Makkovik, and southern Nain provinces along the Lithoprobe ECSOOT Transect: regional seismic refraction and gravity models and their tectonic implications. Can. J. Earth Sci. 35, 583–601.
McCaffrey, K.J.W., Grocott, J., Garde, A.A., Hamilton, M.A., 2004. Attachment formation during partitioning of oblique convergence in the Ketilidian orogen, South Greenland. Geol. Soc. Lond. Spec. Publ. 227, 231–248.
Menke, W., 1989. Geophysical Data Analysis: Discrete Inverse Theory. Academic Press.
Mordret, A., 2018. Uncovering the Iceland hot spot track beneath Greenland. J. Geophys. Res. Solid Earth 123, 4922–4941.
Nielsen, T.K., Larsen, H.C., Hopper, J.R., 2002. Contrasting rifted margin styles south of Greenland: implications for mantle plume dynamics, *Earth Planet.* Sci. Lett. 200, 271–286. https://doi.org/10.1016/S0012-821X(02)00616-7.
Oakey, G.N., Chalmers, J.A., 2012. A new model for the Paleogene motion of Greenland relative to North America: Plate reconstructions of the Davis Strait and Nares Strait regions between Canada and Greenland. J. Geophys. Res. 117 https://doi.org/10.1029/2011JB008942.
Ottemöller, L., Midzi, V., 2003. The crustal structure of Norway from inversion of teleseismic receiver functions. J. Seismol. 7, 35–48. https://doi.org/10.1023/A:1021294504092.
Owens, T.J., Taylor, S.R., Zandt, G., 1987. Crustal structure at regional seismic test network stations determined from inversion of broadband teleseismic P waveforms. Bull. Seismol. Soc. Am. 77, 631–662.
Peace, A.L., 2021. Beyond 'crumple zones': recent advances, applications and future directions in deformable plate tectonic modelling. Geol. Mag. 158, 1704–1710. https://doi.org/10.1017/S0016756821000534.
Peace, A., McCaffrey, K., Imber, J., Phethean, J., Nowell, G., Gerdes, K., Dempsey, E., 2016. An evaluation of Mesozoic rift-related magmatism on the margins of the Labrador Sea: Implications for rifting and passive margin asymmetry. Geosphere 12, 1701–1724. https://doi.org/10.1130/GES01341.1.
Peace, A.L., Foulger, G.R., Schiffer, C., McCaffrey, K.J., 2017. Evolution of Labrador Sea–Baffin Bay: Plate or Plume Processes? Geosci. Can. 44 (3), 91–102.
Peace, A.L., Dempsey, E., Schiffer, C., Welford, J., McCaffrey, K., Imber, J., Phethean, J., 2018a. Evidence for Basement Reactivation during the opening of the Labrador Sea from the Makkovik Province, Labrador, Canada: Insights from Field Data and Numerical Models. Geosciences 8, 308.
Peace, A.L., McCaffrey, K., Imber, J., Hunen, J., Hobbs, R., Wilson, R., 2018b. The role of pre-existing structures during rifting, continental breakup and transform system development, offshore West Greenland. Basin Res. 30, 373–394. https://doi.org/10.1111/bre.12257.
Peace, A.L., Phethean, J.J.J., Franke, D., Foulger, G.R., Schiffer, C., Welford, J.K., McHone, G., Rocchi, S., Schnabel, M., Doré, A.G., 2020. A review of Pangaea dispersal and large Igneous Provinces – in search of a causative mechanism. Earth-Sci. Rev. 206, 102902 https://doi.org/10.1016/j.earscirev.2019.102902.
Péron-Pinvidic, G., Manatschal, G., 2009. The final rifting evolution at deep magma-poor passive margins from Iberia-Newfoundland: a new point of view. Int. J. Earth Sci. 98, 1581–1597. https://doi.org/10.1007/s00531-008-0337-9.
Petersen, K.D., Schiffer, C., 2016. Wilson cycle passive margins: Control of orogenic inheritance on continental breakup. Gondwana Res. 39, 131–144. https://doi.org/10.1016/j.gr.2016.06.012.
Petersen, K.D., Schiffer, C., Nagel, T., 2018. LIP formation and protracted lower mantle upwelling induced by rifting and delamination. Sci. Rep. 8, 16578. https://doi.org/10.1038/s41598-018-34194-0.
Piepjohn, K., von Gosen, W., Tessensohn, F., 2016. The Eurekan deformation in the Arctic: an outline. J. Geol. Soc. jgs2016-081 https://doi.org/10.1144/jgs2016-081.
Postlethwaite, B., Bostock, M.G., Christensen, N.I., Snyder, D.B., 2014. Seismic velocities and composition of the Canadian crust. Tectonophysics 633, 256–267. https://doi.org/10.1016/j.tecto.2014.07.024.
Pourpoint, M., Anandakrishnan, S., Ammon, C.J., Alley, R.B., 2018. Lithospheric structure of Greenland from ambient noise and earthquake surface wave tomography. J. Geophys. Res. Solid Earth 123, 7850–7876.
Reid, I., 1996. Crustal structure across the Nain–Makkovik boundary on the continental shelf off Labrador from seismic refraction data. Can. J. Earth Sci. 33, 460–471.
Reid, I., Jackson, H.R., 1997. Crustal structure of northern Baffin Bay: Seismic refraction results and tectonic implications. J. Geophys. Res. Solid Earth 102, 523–542. https://doi.org/10.1029/96JB02656.
Rondenay, S., 2009. Upper Mantle Imaging with Array Recordings of Converted and Scattered Teleseismic Waves. Surv. Geophys. 30, 377–405. https://doi.org/10.1007/s10712-009-9071-5.
Rondenay, S., Spieker, K., Sawade, L., Halpaap, F., Farestveit, M., 2017. Glimer: a new global database of teleseismic receiver functions for imaging earth structure. Seismol. Res. Lett. 88, 39–48.
Rychert, C.A., Rondenay, S., Fischer, K.M., 2007. P-to-S and S-to-P imaging of a sharp lithosphere-asthenosphere boundary beneath eastern North America. J. Geophys. Res. Solid Earth 112.
Sandvol, E., Seber, D., Barazangi, M., Vernon, F., Mellors, R., Al-Amri, A., 1998. Lithospheric seismic velocity discontinuities beneath the Arabian Shield. Geophys. Res. Lett. 25, 2873–2876. https://doi.org/10.1029/98GL02214.
Schiffer, C., Nielsen, S.B., 2016. Implications for anomalous mantle pressure and dynamic topography from lithospheric stress patterns in the North Atlantic Realm. J. Geodyn. 98, 53–69. https://doi.org/10.1016/j.jog.2016.03.014.
Schiffer, C., Jacobsen, B.H., Balling, N., Ebbing, J., Nielsen, S.B., 2015a. The East Greenland Caledonides—teleseismic signature, gravity and isostasy. Geophys. J. Int. 203, 1400–1418. https://doi.org/10.1093/gji/ggv373.
Schiffer, C., Stephenson, R.A., Petersen, K.D., Nielsen, S.B., Jacobsen, B.H., Balling, N., Macdonald, D.I.M., 2015b. A sub-crustal piercing point for North Atlantic reconstructions and tectonic implications. Geology 43, 1087–1090. https://doi.org/10.1130/G37245.1.
Schiffer, C., Balling, N., Ebbing, J., Jacobsen, B.H., Nielsen, S.B., 2016a. Geophysical-petrological modelling of the East Greenland Caledonides – Isostatic support from crust and upper mantle. Tectonophysics 692, 44–57. https://doi.org/10.1016/j.tecto.2016.06.023.
Schiffer, C., Stephenson, R., Oakey, G.N., Jacobsen, B.H., 2016b. The crustal structure of Ellesmere Island, Arctic Canada—teleseismic mapping across a remote intraplate orogenic belt. Geophys. J. Int. 204, 1579–1600. https://doi.org/10.1093/gji/ggv539.
Schiffer, C., Tegner, C., Schaeffer, A.J., Pease, V., Nielsen, S.B., 2018. High Arctic geopotential stress field and implications for geodynamic evolution. Geol. Soc. Lond. Spec. Publ. 460, 441–465.
Schiffer, C., Eken, T., Rondenay, S., Taymaz, T., 2019. Localized crustal deformation along the central North Anatolian Fault Zone revealed by joint inversion of P-receiver functions and P-wave polarizations. Geophys. J. Int. 217, 682–702. https://doi.org/10.1093/gji/ggz040.
Schiffer, C., Doré, A.G., Foulger, G.R., Franke, D., Geoffroy, L., Gernigon, L., Holdsworth, B., Kusznir, N., Lundin, E., McCaffrey, K., Peace, A.L., Petersen, K.D., Phillips, T.B., Stephenson, R., et al., 2020. Structural inheritance in the North Atlantic. Earth-Sci. Rev. 206, 102975 https://doi.org/10.1016/j.earscirev.2019.102975.
Schmidt, J., 2000. Deep Seismic Studies in the Western Part of the Baltic Shield.
Schulte-Pelkum, V., Mahan, K.H., Shen, W., Stachnik, J.C., 2017. The distribution and composition of high-velocity lower crust across the continental U.S.: Comparison of seismic and xenolith data and implications for lithospheric dynamics and history. Tectonics 36, 1455–1496. https://doi.org/10.1002/2017TC004480.
Scott, D.J., 1998. An overview of the U-Pb geochronology of the Paleoproterozoic Torngat Orogen, Northeastern Canada. Precambrian Res. 91, 91–107. https://doi.org/10.1016/S0301-9268(98)00040-0.
Skaarup, N., Jackson, H.R., Oakey, G., 2006. Margin segmentation of Baffin Bay/Davis Strait, eastern Canada based on seismic reflection and potential field data. Mar. Pet. Geol. 23, 127–144.
Stephenson, R., Piepjohn, K., Schiffer, C., Gosen, W.V., Oakey, G.N., Anudu, G., 2017. Integrated crustal–geological cross-section of Ellesmere Island. Geol. Soc. Lond. Spec. Publ. 460 (SP460), 12. https://doi.org/10.1144/SP460.12.
St-Onge, M.R., Van Gool, J.A., Garde, A.A., Scott, D.J., 2009. Correlation of Archaean and Palaeoproterozoic units between northeastern Canada and western Greenland: constraining the pre-collisional upper plate accretionary history of the Trans-Hudson orogen. Geol. Soc. Lond. Spec. Publ. 318, 193–235.
Storey, M., Duncan, R.A., Pedersen, A.K., Larsen, L.M., Larsen, H.C., 1998. 40Ar/39Ar geochronology of the West Greenland Tertiary volcanic province, *Earth Planet.* Sci. Lett. 160, 569–586.
Suckro, S.K., Gohl, K., Funck, T., Heyde, I., Ehrhardt, A., Schreckenberger, B., Gerlings, J., Damm, V., Jokat, W., 2012. The crustal structure of southern Baffin Bay: Implications from a seismic refraction experiment. Geophys. J. Int. 190, 37–58. https://doi.org/10.1111/j.1365-246X.2012.05477.x.
Suckro, S.K., Gohl, K., Funck, T., Heyde, I., Schreckenberger, B., Gerlings, J., Damm, V., 2013. The Davis strait crust-a transform margin between two oceanic basins. Geophys. J. Int. 193, 78–97. https://doi.org/10.1093/gji/ggs126.
Svenningsen, L., Jacobsen, B.H., 2007. Absolute S-velocity estimation from receiver functions. Geophys. J. Int. 170, 1089–1094. https://doi.org/10.1111/j.1365-246X.2006.03505.x.
Tappe, S., Foley, S.F., Stracke, A., Romer, R.L., Kjarsgaard, B.A., Heaman, L.M., Joyce, N., 2007. Craton reactivation on the Labrador Sea margins: 40Ar/39Ar age and Sr–Nd–Hf–Pb isotope constraints from alkaline and carbonatite intrusives. Earth Planet. Sci. Lett. 256, 433–454. https://doi.org/10.1016/j.epsl.2007.01.036.
Tarantola, A., Valette, B., 1982. Generalized nonlinear inverse problems solved using the least squares criterion. Rev. Geophys. 20, 219–232. https://doi.org/10.1029/RG020i002p00219.
Thompson, D.A., Bastow, I.D., Helffrich, G., Kendall, J.-M., Wookey, J., Snyder, D.B., Eaton, D.W., 2010. Precambrian crustal evolution: Seismic constraints from the Canadian Shield. Earth Planet. Sci. Lett. 297, 655–666. https://doi.org/10.1016/j.epsl.2010.07.021.
Thompson, D.A., Kendall, J.-M., Helffrich, G.R., Bastow, I.D., Wookey, J., Snyder, D.B., 2015. CAN-HK: an a Priori Crustal Model for the Canadian Shield. Seismol. Res. Lett. 86, 1374–1382. https://doi.org/10.1785/0220150015.
Thybo, H., Artemieva, I.M., 2013. Moho and magmatic underplating in continental lithosphere. Tectonophysics 609, 605–619. https://doi.org/10.1016/j.tecto.2013.05.032.
Van Gool, J.A.M., Connelly, J.N., Marker, M., Mengel, F.C., 2002. The Nagssugtoqidian Orogen of West Greenland: tectonic evolution and regional correlations from a West Greenland perspective. Can. J. Earth Sci. 39, 665–686. https://doi.org/10.1139/e02-027.
Vervaet, F., Darbyshire, F., 2022. Crustal structure around the margins of the eastern Superior craton, Canada, from receiver function analysis. Precambrian Res. 368, 106506.

Vinnik, L.P., 1977. Detection of waves converted from P to SV in the mantle. Phys. Earth Planet. Inter. 15, 39–45. https://doi.org/10.1016/0031-9201(77)90008-5.
Wardle, R.J., Gower, C.F., James, D.T., St-Onge, M.R., Scott, D.J., Garde, A.A., Culshaw, N.G., van Gool, J.A., Connelly, J.N., Perreault, S., 2002. Correlation chart of the Proterozoic assembly of the northeastern Canadian-Greenland Shield. Can. J. Earth Sci. 39, 895.
Welford, J.K., Hall, J., 2013. Lithospheric structure of the Labrador Sea from constrained 3-D gravity inversion. Geophys. J. Int. 195, 767–784.
Welford, J.K., Peace, A.L., Geng, M., Dehler, S.A., Dickie, K., 2018. Crustal structure of Baffin Bay from constrained three-dimensional gravity inversion and deformable plate tectonic models. Geophys. J. Int. 214, 1281–1300. https://doi.org/10.1093/gji/ggy193.
Whitmeyer, S., Karlstrom, K.E., 2007. Tectonic model for the Proterozoic growth of North America. Geosphere 3, 220. https://doi.org/10.1130/GES00055.1.
Wilson, R.W., Klint, K.E.S., van Gool, J.A., McCaffrey, K.J., Holdsworth, R.E., Chalmers, J.A., 2006. Faults and fractures in central West Greenland: onshore expression of continental break-up and sea-floor spreading in the Labrador–Baffin Bay Sea. Geol. Surv. Den. Greenl. Bull. 11, 185–204.
Wilton, D.H.C., Taylor, R.C., Sylvester, P.J., Penney, G.T., 2002. A review of kimberlitic and ultramafic lamprophyre intrusives from northern Labrador. Curr. Res. Nfld Dep. Mines Energy Geol. Surv. Rep. 2, 343–352.
Wilton, D., Burden, E., Greening, A., 2016. The Ford's Bight Diatreme a Cretaceous Alnöite Pipe from the Northern Labrador Coast and Possible Onland Remnant from the Opening of the Labrador Sea. In: Arctic Technology Conference, Offshore Technology Conference.